sensors

MDPI

Article

An Ultra-Low-Cost RCL-Meter

Pedro M. C. Inácio [1], Rui Guerra [1,2,*] and Peter Stallinga [1,3]

[1] CEOT—Center for Electronics, Optoelectronics and Telecommunications, University of Algarve, Campus Gambelas, 8005-139 Faro, Portugal; pminacio@ualg.pt (P.M.C.I.); pjotr@ualg.pt (P.S.)
[2] Department of Physics, University of Algarve, Campus Gambelas, 8005-139 Faro, Portugal
[3] Department of Electronics and Computer Engineering, University of Algarve, Campus Gambelas, 8005-139 Faro, Portugal
* Correspondence: rguerra@ualg.pt

Abstract: An ultra-low-cost RCL meter, aimed at IoT applications, was developed, and was used to measure electrical components based on standard techniques without the need of additional electronics beyond the AVR® micro-controller hardware itself and high-level routines. The models and pseudo-routines required to measure admittance parameters are described, and a benchmark between the ATmega328P and ATmega32U4 AVR® micro-controllers was performed to validate the resistance and capacitance measurements. Both ATmega328P and ATmega32U4 micro-controllers could measure isolated resistances from 0.5 Ω to 80 MΩ and capacitances from 100 fF to 4.7 mF. Inductance measurements are estimated at between 0.2 mH to 1.5 H. The accuracy and range of the measurements of series and parallel RC networks are demonstrated. The relative accuracy (a_r) and relative precision (p_r) of the measurements were quantified. For the resistance measurements, typically a_r, p_r < 10% in the interval 100 Ω–100 MΩ. For the capacitance, measured in one of the modes (fast mode), a_r < 20% and p_r < 5% in the range 100 fF–10 nF, while for the other mode (transient mode), typically a_r < 20% in the range 10 nF–10 mF and p_r < 5% for 100 pF–10 mF. a_r falls below 5% in some sub-ranges. The combination of the two capacitance modes allows for measurements in the range 100 fF–10 mF (11 orders of magnitude) with a_r < 20%. Possible applications include the sensing of impedimetric sensor arrays targeted for wearable and in-body bioelectronics, smart agriculture, and smart cities, while complying with small form factor and low cost.

Keywords: impedance meter; RCL-bridges; portable instrument; AVR® micro-controller; low-cost; internet of things

check for updates

Citation: Inácio, P.M.C.; Guerra, R.; Stallinga, P. An Ultra-Low-Cost RCL-Meter. *Sensors* **2022**, *22*, 2227. https://doi.org/10.3390/s22062227

Academic Editors: Alexandru Lavric, Liliana Anchidin and Adrian I. Petrariu

Received: 18 January 2022
Accepted: 8 March 2022
Published: 14 March 2022

Publisher's Note: MDPI stays neutral with regard to jurisdictional claims in published maps and institutional affiliations.

Copyright: © 2022 by the authors. Licensee MDPI, Basel, Switzerland. This article is an open access article distributed under the terms and conditions of the Creative Commons Attribution (CC BY) license (https://creativecommons.org/licenses/by/4.0/).

1. Introduction

The Internet of Things (IoT) entails a network of physical objects—'things'—that are embedded with sensors, electronics, software, etc. for the purpose of communicating with other devices over the Internet. Caused by the sheer number of things connected in this way, these data-acquisition devices obviously need to be of low-cost and fulfill certain tasks: sensing, electronic processing and connecting to the Internet. Impedimetric sensor arrays are an emerging field of study that is concerned with sense, processing and casting the measured data to the Internet [1–3]. Typical applications are wearable and in-body electronics [4–8] and plants and smart agriculture [9–13]. A common aspect shared between different devices is that the electronic interfaces for detection, processing and connection to the Internet are mainly carried out by separate external systems specifically optimized for each of these functions. While designing a system with specific units may often be advantageous to enhance the overall performance of the device, it also leads to higher manufacturing cost. For example, most biosensors feature a transduction mechanism to couple the physical and/or chemical changes in the system under measurement to the electronic circuitry of the measuring device. The latter is specifically optimized for the sensing interface and is followed by an analog-to-digital conversion unit (ADC). In the most usual scenario, the end

user has access to a plug-and-play instrument box. But even in this case, the transduction mechanism may require finding signal conditioning strategies in order to maximize the linear range of the analog signal and the corresponding measurement accuracy [14–17].

Furthermore, the measurement unit, which often replaces a benchtop instrument, must be designed for small form factor devices and a low power profile, while maintaining performance close to gold standard instruments. Application-specific integrated circuit (ASIC) based devices fulfill these requirements, such as the ones developed to perform online electrochemical impedance spectroscopy (EIS) for characterization of lithium-ion battery packs [18–20]. This technology can be extended to other applications in areas where size and power consumption are crucial. For instance, in our research we have been developing technology for using admittance spectroscopy to determine the physical state of plants [21]. However, this study relied on bulky and expensive lock-in detectors, not appropriate for an IoT implementation. A cheaper solution developed by S. Grassini is to use an Arduino-based electrochemical impedance spectroscopy (EIS) system [22] for in situ corrosion monitoring of metallic works of art [23]. The Arduino-based EIS is already a huge improvement over conventionally used RCL-bridges (resistance, capacitance, inductance) and lock-in detectors. Similarly, the ASIC-based miniaturized system for Online-EIS proposed by Manfredini [19] shows how versatile the ASIC device is, being capable of measuring not only the impedance of commercial batteries, but also capacitive and resistive sensors. The device is based on the SENSIPLUS, which is a System on a Chip (SoC) solution that uses minimal external hardware, and shows performance on a par with gold standard instruments. The Arduino has been also used as a platform to measure capacitances, as explained, for example, by Campbell [24]. It has been used to deploy a digital LCR meter [25] to measure single parameters (not combinations), although this depends on the known nominal values of external components.

The current report describes a very-low-cost solution for an admittance meter, resulting from an effort to lower the cost and the size of these instruments. Specifically, it uses a micro-controller for directly measuring admittance without the need for any additional electronic circuitry beyond the micro-controller hardware itself. The proposed implementation differs from the instruments developed by [22,24] in two main features: (i) it is based on a time-domain approach, since the measurements are performed with signal transients rather than with sinusoidal signals; (ii) it avoids the need for external circuits, since all the signal generation and detection are performed by the micro-controller. Moreover, when used in popular platforms such as Arduino, full functionality is available, from sensing to communicating, for a price that lies in the order of mere euros per unit, thus fulfilling the requirement of the Internet of Things. Additionally, it paves the way to cheaper wearable and in-body bioelectronic sensors, allowing a live feed of collected data from impedimetric sensor arrays to the IoT, constituting an all-in-one solution: Sensing, Processing and Connection to the Internet. The technique that we will describe here relies on determining the behavior after applying voltage steps, a standard technique used in circuit analysis, which can readily measure resistances and capacitances, either isolated or in series and parallel. It is based on the low-cost AVR® micro-controller series commonly used in the Arduino® platform. The accuracy and precision of the measurements are discussed based on the relative parameters of measurement uncertainty (u_r), accuracy (a_r) and precision (p_r). All the C++ codes for Arduino and the MATLAB scripts used in this manuscript are available in the Supplementary Materials.

2. Materials and Methods

2.1. AVR® Micro-Controllers Based RCL-Meter

Two development boards manufactured by Arduino®, namely the Uno and Leonardo boards, were used to develop the ultra-low-cost RCL-meter. The Arduino® Uno board makes use of an ATmega328P micro-controller, and the Arduino® Leonardo uses an ATmega32U4. Figure 1e shows the block diagram of the proposed measurement system based exclusively on the internal circuitry of the AVR® micro-controller. Both ATmega328P [26] and ATmega32U4 [27] are low-power AVR® 8-bit micro-controllers that share similar fea-

tures, namely equal clock frequency up to 16 MHz, operational voltage range between 2.7 to 5.5 V, 32 kB of flash memory (enough to store the firmware and processing code), 2 kB (ATmega328P)/2.5 kB (ATmega32U4) of static random-access memory (SRAM) (to store the main variables and acquisition samples) and an analog-to-digital unit (ADC) with 10-bit resolution, the core of the system. Both the Uno and Leonardo boards were supplied through the local-PC connection via USB interface, and the default settings were used, meaning the reference voltage (V_{REF}) is the internal voltage source of 5 V.

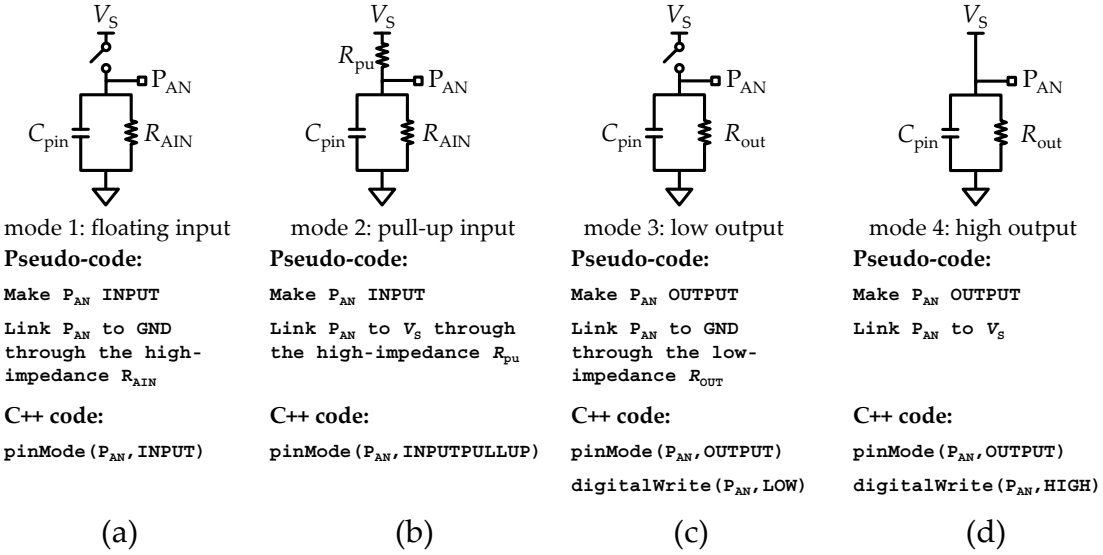

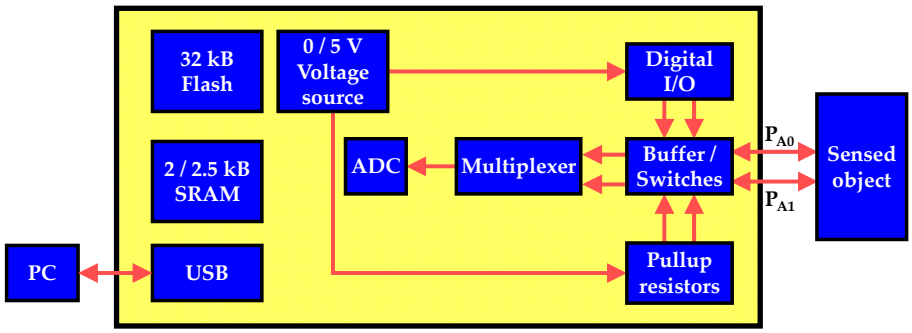

(e)

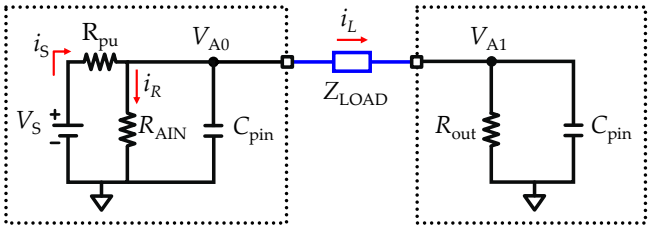

(f)

Figure 1. Equivalent circuits for the four operation modes available to configure each analog input/output (I/O) port. (**a**) mode 1, floating input. (**b**) mode 2, pull-up input. (**c**) mode 3, low output. (**d**) mode 4, high output. Each equivalent circuit is adapted from the schematics provided in the datasheets. (**e**) Block diagram of the proposed measurement system, including the serial communication and voltage source through USB interface to local PC, flash and SRAM memory, internal voltage source, and internal circuitry to program I/O ports to digital or alternate functionalities. (**f**) Equivalent circuit of two analog I/O ports bridged with a load impedance (Z_{LOAD}).

2.2. Analog I/O Operation Modes

The AVR® micro-controller family provides access to several digital and analog ports with input and output (I/O) functionalities. Both digital and analog I/O ports share a common control unit design, often called "General Digital I/O" [26,27]. In this work, the digital I/O ports (PDN) are labeled by an alpha-numerical code, denoted by the letter "D" proceeded by the port bit number "N", while the analog I/O ports (PAN) are represented by the letter "A". The analog ports have exclusive access to the alternate functions, featuring an I/O source-measuring unit (SMU) and an analog-to-digital converter (ADC) unit. By default, P_{AN} ports can be configured into four distinct operation modes: (mode 1) floating input; (mode 2) pull-up input; (mode 3) low voltage output; (mode 4) high voltage output. Each operation mode shares the same basic electrical structure, consisting of the supply voltage source (V_S), common ground (GND), a stray capacitance (C_{pin}) and location of the I/O port (P_{An}) for the SMU and ADC unit. By default, vs. is equal to the reference voltage (V_{REF}). Figure 1 shows the equivalent circuit that describes each analog I/O port operation mode and was adapted from references [26,27]. Operation modes 1 and 2, shown in Figure 1a,b, respectively, share the same internal circuitry components to form a high-impedance input port due to the presence of the analog input resistance (R_{AIN}). C_{pin} is also included in parallel with R_{AIN} to account for the stray capacitance. The unique difference between operation mode 1 and 2 is the state of the internal pull-up resistance (R_{pu}), which is connected to an internal bias voltage. In the case of operating mode 1, the R_{pu} is inactive, leading to a floating input configuration, while in the case of operation mode 2, the R_{pu} sets a SMU configuration. This aspect will be further explored to implement the RCL-meter. Operation modes 3 and 4, shown in Figure 1c,d, relate to the "General Digital I/O" functions. Operation mode 3 consists of a floating and impedance low output configuration, and the operation mode 4 consists of a voltage source (V_S), thus forcing a high output configuration. In the absence of load impedance connected to P_{AN}, the configuration of the operation mode 4 sinks current through the parallel RC network formed by the output resistance (R_{out}) and C_{pin}. Table 1 shows the typical values of the internal components of the I/O ports [26,27].

Table 1. Typical values of the operational voltage of the circuits (V_S), the ADC unit, the internal circuitry to each I/O port and the TTL unit to each AVR® micro-controller [26,27].

Voltage Source	ADC Unit		Internal Circuitry Parameters				TTL Unit			
							ATmega328P		ATmega32U4	
V_S (V)	n	N_{max} $(2^n - 1)$	R_{AIN} (MΩ)	R_{out} (Ω)	R_{pu} (kΩ)	C_{pin} (pF)	V_{IL} (V)	V_{IH} (V)	V_{IL} (V)	V_{IH} (V)
5	10	1023	100	600	32	24	−0.5–1.5	3.0–5.5	−0.5–0.9	1.9–5.5

The R_{pu} and C_{pin} values listed in Table 1 are representative values. In case of the R_{pu}, both micro-controller datasheets [26,27] characterize the range of R_{pu} between 20 kΩ to 50 kΩ, and solely for the purpose of the ADC unit it refers a typical reference input resistance (R_{REF}) value of 32 kΩ. As for the C_{pin}, the micro-controller datasheets [26,27] do not provide a typical value; only a conceptual component is shown in the equivalent circuits of the analog input circuitry representing the overall stray capacitance (also named C_{pin}). Therefore, the typical stray capacitance listed in Table 1 considers all capacitive sources in the internal analog input circuitry, such as: (i) the sampling and holder capacitance ($C_{S/H}$), approximately equal to 14 pF and (ii) the input capacitance (C_i) of each I/O pin, approximately equal to 10 pF. Both $C_{S/H}$ and C_i are grounded; therefore, it is assumed that the parallel of both $C_i \parallel C_{S/H}$ is the minimum value of C_{pin} and is approximately equal to $C_{pin} \cong C_i \parallel C_{S/H} \cong 24$ pF.

In practical terms, the operation mode of each port available on an AVR® micro-controller must be configured according to the pseudo-code described in Figure 1 through a low-level instruction set, which is not a user-friendly environment. However, Arduino®

has developed an integrated development environment (IDE) platform with support of high-level C++ functions such as pinMode() and digitalWrite(), an easy and user-friendly method to configure the ports. Figure 1 describes the C++ code required to properly configure each operation mode. In the following sections, it will be shown how the four different configurations for the ports may be used to build an RCL bridge. First, it is shown how to measure isolated resistors, capacitors and inductors, and then how to measure combinations of resistors and capacitors in series or parallel.

2.3. Recording Circuit

The recording circuit to measure resistances, capacitances and inductances, either isolated or in series and parallel is composed of the same internal components by setting two I/O ports with alternate functions, namely P_{A0} and P_{A1} ports configured for pull-up input (mode 1) and low output (mode 3), respectively, and as described in Section 2.2. Figure 1f shows the equivalent circuit resulting from the combination of the internal circuitry of each I/O port bridged by a load impedance (Z_{LOAD}). In the following Sections 2.4–2.8, the equivalent circuit shown in Figure 1f is detailed by replacing Z_{LOAD} with resistance, capacitance and inductance, either isolated or in series and parallel.

2.4. Measurements of an Isolated Load Resistance (R–Meter)

Considering that in the equivalent circuit shown in Figure 1f, Z_{LOAD} is composed of an isolated load resistance (R_{LOAD}), the pull-up resistor (R_{pu}) at port P_{A0} drives a current source that will sink through the parallel resistance path (R_P) formed by the analog input resistance (R_{AIN}) and the sum of the load and output resistances (R_{LOAD} + R_{out}). Thus, for circuit analysis purposes, in Figure 2a, a reduction of the entire equivalent circuit to a voltage divider circuit is shown. In Figure 2a, the variable N_{A0} is introduced as the digital counterpart of the analog variable $V_{A0,}$ where $N_{A0} = \lfloor N_{max} \cdot (V_{A0}/V_S) \rfloor$. The stray capacitances (C_{pin}) were neglected from the equivalent circuit, since on DC measurements, the capacitances behave as open circuit. In addition, to avoid interference of any stray capacitance, the procedure is to implement a reasonable delay time (say 1 ms) after setting the port P_{A0} to operation mode 2 (pullup input). This procedure assures that the stray capacitances are open circuit ($t \gg \tau = R_T C_{pin}$). Using C_{pin} = 25 pF and R_{pu} = 32 kΩ, one obtains $\tau < 1$ µs.

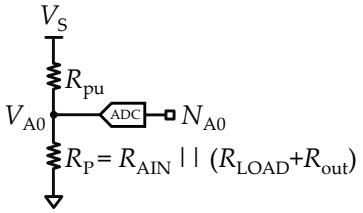

(a)

Pseudo-code:

```
Set port P_A0 to INPUT PULLUP
Set port P_A1 to LOW OUTPUT
Sample port P_A0:
  NA0 measures V_A0
R_LOAD is given by Eq.(2)
```

(b)

Figure 2. Set-up of a pure load resistance meter (R-meter). (**a**) Reduction of the equivalent circuit to a voltage divider circuit. (**b**) Pseudo-code used to implement the resistance meter mode.

In Figure 2a, V_{A0} is the measured voltage at port P_{A0} and is given by:

$$V_{A0} = V_S \frac{R_p}{R_{pu} + R_p} \tag{1}$$

where R_P is given by R_{AIN} || (R_{LOAD} + R_{out}), and vs. is equal to the reference voltage source (V_{REF}). Solving the voltage divider Equation (1), R_{LOAD} is found as:

$$R_{LOAD} = \frac{R_{AIN}R_{out} - K(R_{AIN} + R_{out})}{K - R_{AIN}}, K = R_{pu}\frac{V_{A0}}{V_S - V_{A0}} \tag{2}$$

where K is an auxiliary variable used to shorten the length of Equation (2). All the parameters described in Equation (2) are known values, and are available on the datasheet of the micro-controller. The pseudo-code for a routine to measure R_{LOAD} is described in Figure 2b.

2.5. Measurements of an Isolated Load Capacitance (C–Meter)

Two methodologies are reported in this section: (i) fast acquisition mode, which is based on the immediate response of the C_{LOAD} charging cycle, and (ii) transient acquisition mode, based on measuring the charging time until a threshold voltage is reached. It is essential that prior to initiating measurements of C_{LOAD}, all capacitive components are fully discharged. A typical procedure to discharge all capacitances is achieved by configuring the operation mode of the two I/O ports in use to low output (mode 3) and waiting, for example, a period of $\Delta t \geq 1$ ms.

2.5.1. Fast Acquisition Mode of an Isolated Load Capacitance

As an exception to all other methods presented in this manuscript, the fast acquisition mode to measure an isolated load capacitance (C_{LOAD}) uses a different internal circuitry. Therefore, Figure 3a shows the equivalent circuit resulting from the combination of the internal circuitry of two I/O ports, P_{A0} and P_{A1}, bridged by a pure load capacitance (C_{LOAD}). Essentially, the port P_{A1} is set in high output (mode 4) and links the voltage source (V_S) to the C_{LOAD} terminal behaving as an input current source (i_S), and the port P_{A0} is set to floating input (mode 1), consisting of a measuring unit that links the input current to the ground through a high impedance resistor (R_{AIN}). Both the P_{A1} and P_{A0} ports consider the leakage current path to the ground through a stray capacitance (C_{pin}). However, the C_{pin} located at P_{A1} can be neglected, since the characteristic time constant (τ_{A1}) of P_{A1} is $\tau_{A1} = R_{out}C_{pin} \cong 15$ ns, and therefore, because the fastest clock cycle (τ_{clk}) of the micro-controllers in use are approximately equal to $\tau_{clk} \approx 5\tau_{A1}$, after a single clock cycle the voltage in port P_{A1} (V_{A1}) is stationary.

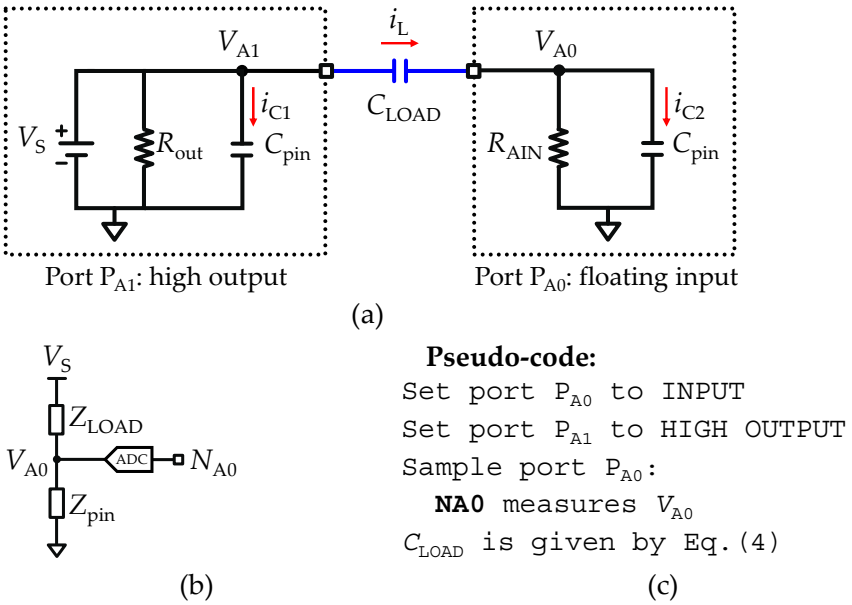

Figure 3. Set-up of a pure load capacitance meter (*C*-meter). (**a**) Equivalent circuit of two analog I/O ports bridged with a load capacitance (C_{LOAD}). (**b**) Reduction of the equivalent circuit to an impedance divider. (**c**) Pseudo-code used to implement the fast acquisition mode.

For circuit analysis purposes, assuming all capacitances are fully discharged at the instant $t = 0$, all capacitances are shorted and all currents flow through the capacitive path. In these circumstances, the circuit analysis is simpler considering that at $t = 0$ the current

path flow exclusively through the capacitive path (C_T) formed by the load (C_{LOAD}) and stray (C_{pin}) capacitors in series, given by $C_T = C_{LOAD}C_{pin}/(C_{LOAD} + C_{pin})$. This allows the reduction of the entire equivalent circuit to a voltage divider, as shown in Figure 3b, and is only valid for measuring the impulse response. Thus, V_{A0} must be read immediately after defining P_{A0} to floating input and P_{A1} to high output.

One approach to find the load capacitance is through the analysis of the charge level (Q) of the circuit. Since both C_{LOAD} and C_{pin} are in series, the charge level must be equal in both capacitances ($Q_{LOAD} = Q_{pin}$), thus allowing the expression of V_{A0} as:

$$V_{A0} = V_S \frac{C_{pin}}{C_{pin} + C_{LOAD}} \tag{3}$$

where the solution given by Equation (3) assumes $Q_{LOAD} = C_{LOAD}\,(V_S - V_{A0})$ and $Q_{pin} = C_{pin}V_{A0}$. Rearranging (3), C_{LOAD} is found as:

$$C_{LOAD} = C_{pin} \frac{V_{A0}}{V_S - V_{A0}} \tag{4}$$

The size of C_{pin} is made available through the datasheet of the micro-controller, and is typically 25 pF, while vs. is equal to the reference voltage source (V_{REF}), and V_{A0} is the measured voltage at port P_{A0}. Thus, all parameters are known, and C_{LOAD} can be determined. Lastly, the fast acquisition mode methodology is limited by the size of the C_{pin}, such that, if $V_{A0} \to N_{max}$, the maximum range of (4) is an asymptote with $C_{LOAD} \to \infty$. Therefore, an approximation to determine the range of measurable C_{LOAD} is:

$$\frac{C_{pin}}{N_{max} - 1} \leq C_{LOAD} \leq C_{pin}(N_{max} - 1) \tag{5}$$

where the total range is obtained for $1 \leq N_{A0} < N_{max} - 1$. The pseudo-code for a routine to measure C_{LOAD} through the fast acquisition mode is described in Figure 3c.

2.5.2. Transient Acquisition Mode of an Isolated Load Capacitance

As pointed out before, the fast-acquisition mode methodology has limitations for large capacitances, thus requiring a different measurement strategy, namely monitoring the transient during the charging cycle of a C_{LOAD} bridging the ports P_{A0} and P_{A1} in the equivalent circuit shown in Figure 1f. The stray capacitances (C_{pin}) are not larger than some tens of pico-Farads (pF) and can therefore be neglected.

The remaining circuit analysis is simpler and is preferably done using the impedance analysis. Figure 4a shows the impedance representation of the equivalent circuit, where Z_{in} represents the impedance due to the pull-up resistance (R_{pu}) at the input port P_{A0}, and Z_{out} is the output impedance formed by the parallel RC network between the analog input resistance (R_{AIN}) and the series RC network ($Z_{LOAD} + R_{out}$). Z_{LOAD} is the impedance representation of the load capacitance (C_{LOAD}). Therefore, an estimation of C_{LOAD} is obtained using the step response of the impedance divider circuit shown in Figure 4b, which is given by:

$$V_{A0}(t) = V_S\left(1 - e^{\frac{-t}{\tau}}\right),\ \tau\ = R_T C_{LOAD} \tag{6}$$

where R_T is the total resistance path contributing for the potential difference on the capacitance terminals given by $R_T = R_{AIN}\ ||\ R_{pu} + R_{out}$. Thus, C_{LOAD} can be found at any time t by rearranging Equation (6) to:

$$C_{LOAD} = \frac{t}{R_T \cdot \ln\left(\frac{V_S}{V_S - V_{A0}(t)}\right)} \tag{7}$$

where t is the time since starting the charging of the capacitance. All parameters in Equation (7) are known except for the time (t). Thus, to find the C_{LOAD} value, the elapsed

time (Δt) must be determined, since $t = 0$ until a threshold voltage (V_{th}) is reached. For instance, solving Equation (6) with $t = \tau$ allows the definition of $V_{th} = (1 - e^{-1})V_S$ and therefore solves Equation (7). The elegant procedure for testing V_{th} makes use of the built-in transistor-transistor logic (TTL) unit to monitor V_{A0} by setting the TTL unit high voltage threshold (V_{IH}) to the V_{th} ($V_{th} = V_{IH}$), allowing not only the avoidance of the computation of the V_{th}, but also the enhancement of the accuracy of the measurement. In practical terms, the elapsed time (Δt) since C_{LOAD} initiates the charging cycle ($t = 0$) until the TTL unit changes to the logical state high '1' ($V_{A1} \geq V_{IH}$) must be measured, as well as proceeding to the reading of V_{A0} using the ADC unit (N_{A0}). Then, C_{LOAD} is found by replacing V_{A0} and t by the measured values of N_{A0} and Δt in Equation (7). Figure 4c depicts the voltage step response of the impedance divider circuit. The highlighted region delimited between the voltage level V_{IH} and vs. represents the operation region where the TTL logic unit changes of logic state low '0' to high '1'. For reference, Table 1 includes the typical values of V_{IH} for the ATmega328P and ATmega32U4 micro-controllers.

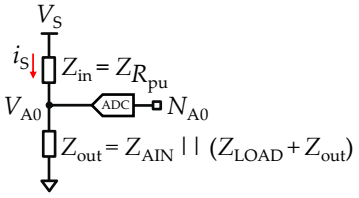

(a)

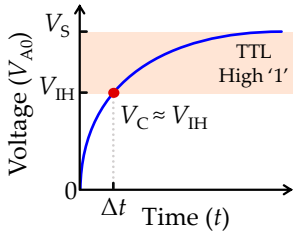

(b)

Pseudo-code:

```
Set port P_A0 and P_A1 to LOW OUTPUT
Wait 1 millisecond: delay (1)
Set port P_A0 to INPUT PULLUP
Read timer: TS measures microseconds
do
  Sample digital port P_A0: NA0 measures V_A0
while (NA0 == 0)
Read timer: TE measures microseconds
Sample port P_A0: NA0 measures V_A0
Determine elapsed time (Δt): T = TE - TS
C_LOAD is given by Eq.(7): Replace V_A0 by NA0
                           t by T
```

(c)

Figure 4. Set-up for recording a pure load capacitance (C_{LOAD}) through the transient acquisition mode. (**a**) Impedance representation of the reduced equivalent circuit. (**b**) Illustration of the step response in voltage measured at the input terminal of C_{LOAD}. V_{IH} is defined in Table 1. (**c**) Pseudo-code used to implement the transient acquisition mode.

Additionally, the transient acquisition mode methodology is limited by the characteristic time constant (τ) of the circuit, such that if $\tau \to 0$, the charging velocity (dv/dt) of the C_{LOAD} increases to proportions where high temporal resolution is required to measure the N_{A0} accurately, since $N_{A0} \to N_{max}$ just before the first reading is taken, causing the ADC unit to overflow. An approximation of the ranging limits of the transient acquisition mode is given by:

$$\frac{\Delta t}{R_T \cdot \ln(N_{max})} \leq C_{LOAD}(t) \leq \frac{\Delta t}{R_T \cdot \ln\left(\frac{N_{max}}{N_{max}-1}\right)} \tag{8}$$

where in Equation (8) the lower and upper resolution of the ADC unit (N_{A0}) are solved assuming $1 \leq N_{A0} \leq N_{max} - 1$. Using the typical values provided in Table 1, the detection limit of the interface assuming the fastest reading of the ADC unit could be achieved after one clock-cycle ($\Delta t = 62.5$ ns). Then, the minimum range of the transient acquisition method varies between 214 fF $\leq C_{min} \leq$ 392 fF with 22.4 kΩ $\leq R_{pu} \leq$ 41.6 kΩ. Nevertheless, the impact of the stray capacitances (C_{pin}) was neglected, and therefore such a range is merely indicative, since $C_{pin} \gg C_{min}$. As for the maximum range of the transient acquisition method, the maximum Δt is limited by the size of the unsigned long variables given by $\Delta t = (2^{32} - 1) \times 1$ µs $\cong$ 4295 s. Thus, the maximum range corresponds to a battery-like storage unit rather than a capacitor, as it is some hundreds of farads. The pseudo-code of a

routine to perform the measurement of C_{LOAD} through the transient acquisition mode is described in Figure 4c.

2.6. Measurements of a Serial RC Network (RC–Meter Mode)

Considering that in the equivalent circuit shown in Figure 1f, Z_{LOAD} is composed by a series RC network, the strategy to extract C_{LOAD} and R_{LOAD} resembles the previously described techniques to measure a pure resistor in Section 2.4 and a pure capacitor through the transient acquisition mode in Section 2.5.2. However, the TTL-based technique used to determine C_{LOAD} cannot guarantee that a TTL transition will occur in the transient response of the circuit, since the voltage V_{A0} might start at a value above the TTL threshold (V_{IH}). Instead, the monitoring process of the transient response must be carried out exclusively using the analog functions available on the AVR® micro-controller ports. First, the C_{LOAD} must be completely discharged, which requires defining both ports P_{A0} and P_{A1} to low output configuration for a reasonable time, and then defining P_{A0} to a high-impedance SMU, while maintaining P_{A1} as low output. For the sake of simplicity, the stray capacitances (C_{pin}) are neglected, which is allowed if they are not larger than some tens of pico-farads (pF).

With C_{LOAD} fully discharged, after setting the port P_{A0} to a high-impedance SMU ($t = 0$), a voltage step is applied on the serial RC circuit. Since C_{LOAD} is empty, it behaves as a short-circuit, which results in an equivalent circuit, as shown in Figure 2a, thus allowing the extraction of the R_{LOAD} value through use of the technique described in Section 2.4 to measure a pure resistor (note that the port configuration is the same). The measured voltage (V_{A0}) at the instant $t = 0$ defines an offset voltage (V_R). For any instant $t > 0$, C_{LOAD} starts to accumulate charge, and the same circuit analysis described in Section 2.5.2 applies to determine the transient dynamics of the voltage step response. For $t \to \infty$, C_{LOAD} is fully charged and behaves as an open circuit, thus forcing the current to flow exclusively through the analog input resistance (R_{AIN}), as represented in Figure 1f by the current path 'i_R'. Thus, considering the influence of the charging current (i_L) due to the series R_{LOAD}, an estimation of C_{LOAD} is obtained using the step response of the equivalent circuit shown in Figure 1f that is given by:

$$V_{A0}(t) = V_R + V_{REF}\left(1 - e^{\frac{-t}{\tau}}\right),\ V_R = \frac{V_S}{R_{pu}} \frac{(R_{out} + R_{LOAD})\left(R_{AIN} \parallel R_{pu}\right)}{R_{out} + R_{LOAD} + R_{AIN} \parallel R_{pu}}, \tag{9}$$

where V_R is the offset voltage due to the series R_{LOAD}, V_{REF} is the new reference voltage of the circuit given by V_{REF} = vs. $- V_R$, τ is the characteristic time constant of the equivalent circuit given by the $\tau = R_T C_{LOAD}$ and R_T is the total resistance path contributing to the potential difference on the capacitance terminals given by $R_T = R_{AIN}$ | | $R_{pu} + R_{LOAD} + R_{out}$. Thus, C_{LOAD} can be found at any time t by rearranging Equation (9) to:

$$C_{LOAD} = \frac{t}{R_T \ln\left(\frac{V_{REF}}{V_{REF} - V_{A0}(t)}\right)} \tag{10}$$

where t is the time that takes charges to accumulate in the capacitance. Figure 5a illustrates the transient response to a voltage step expressed by Equation (10), where the highlighted region consists of the offset voltage (V_R) due to the bridge of ports P_{A0} and P_{A1} with the serial RC network. As for the reading capacitance voltage level (V_C) it is determined when $t = \tau = R_T C_{LOAD}$, and is given by $V_C = V_R + (1 - e^{-1})(V_S - V_R)$. Therefore, all parameters in Equation (10) are known except for the time (t). To extract C_{LOAD}, a routine to determine the elapsed time (Δt) until the measured voltage (V_{A1}) is greater than or equal to V_C ($V_{A0} \geq V_C$) must be implemented. Figure 5b depicts the pseudo-code of a routine to implement the measurement of a serial RC network. In practical terms, C_{LOAD} is found by replacing in Equation (10) V_R with the measured value of N_{A0} at $t = 0$ (N_R), vs. with the maximum resolution of the ADC unit (N_{max}) and V_{A0} and t with the measured value of N_{A0} and Δt after $V_{A0} \geq V_C$, respectively.

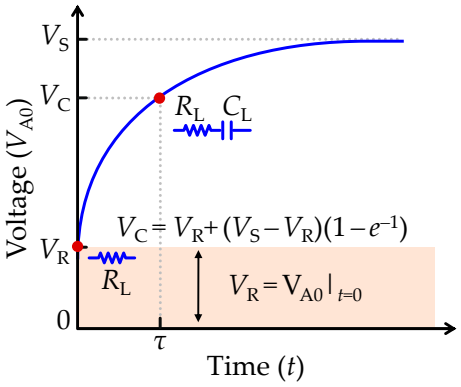

(a)

Pseudo-code:

```
Set port P_A0 and P_A1 to LOW OUTPUT
Wait 1 millisecond: delay (1)
Set port P_A0 to INPUT PULLUP
Sample port P_A0: VR measures V_A0
Read timer: TS measures microseconds
Define stop condition:
  VTAU = VR + 0.6322 × (VS - VR)
do
  Sample port P_A0: VC measures V_A0
while (VC <= VTAU)
Read timer: TE measures microseconds
Determine elapsed time (Δt): T = TE - TS
R_LOAD is given by Eq.(2) : Replace V_A0 by VR
C_LOAD is given by Eq.(10): Replace V_A0 by VC
                            t by T
```

(b)

Figure 5. Set-up for recording a load impedance (Z_{LOAD}) formed by a serial RC network. (**a**) Illustration of the transient response to a voltage step at the input terminal (P_{A0}). (**b**) Pseudo-code used to implement the measurement of a serial RC network.

2.7. Measurements of a Parallel RC Network (RC–Meter Mode)

Considering that in the equivalent circuit shown in Figure 1f, Z_{LOAD} is composed of a parallel RC network ($C_{LOAD} \| R_{LOAD}$), the strategy to extract C_{LOAD} and R_{LOAD} resembles the previously described technique in Section 2.6, although it must be noted that the change of the load capacitance (C_{LOAD}) from serial mode to parallel mode causes R_{LOAD} to saturate at the reference voltage ($V_F = V_R$) level when $t \to \infty$ and the voltage offset is null at $t = 0$. Thus, the step response of the equivalent circuit shown in Figure 1f is given by:

$$V_{A0}(t) = V_F\left(1 - e^{\frac{-t}{\tau}}\right), \tag{11}$$

where V_F is given by the expression of V_R that is defined in Equation (9), τ is the characteristic time constant of the equivalent circuit given by $\tau = R_T C_{LOAD}$ and R_T is the total resistance path given by $R_T = (R_{AIN} \,||\, R_{pu}) \,||\, (R_{LOAD} + R_{out})$. Figure 6a illustrates the transient response to a voltage step expressed by Equation (11). For $t \to \infty$, C_{LOAD} is fully charged and behaves as an open circuit, forcing the current (i_L) represented in the equivalent circuit shown in Figure 1f to flow exclusively through the R_{LOAD} to the ground. Therefore, the extraction of R_{LOAD} is analytically indeterminate, unless an approximation is made, such as, considering for any period (Δt) larger than five times the characteristic time constant (τ) ($\Delta t > 5\tau$), Equation (11) is approximately equal to $V_{A0} = V_F(1 - e^{-5}) \approx V_F$, where the term $(1 - e^{-5}) \approx 0.993$ shows that the approximation has a maximum error of 0.7% when determining the R_{LOAD} value. Thereby, assuming for any $\Delta t > 5\tau$ the plateau $V_{A0} = V_F$ is reached, the R_{LOAD} value is obtained using the technique described in Section 2.4 to measure a pure resistor, replacing in Equation (2) V_{A0} by V_F, where V_F is the measured voltage for any instant $\Delta t > 5\tau$. The next step is to determine the C_{LOAD} value through the arrangement of Equation (11) with $\tau = R_T C_{LOAD}$ by:

$$C_{LOAD} = \frac{t}{R_T \cdot \ln\left(\frac{V_F}{V_F - V_{A0}(t)}\right)} \tag{12}$$

where t is any instant of the step-response and V_{A0} the correspondent measured voltage. The determination of V_F is critical to find both C_{LOAD} and R_{LOAD} values. The simplest approach to find V_F using the transient response to a voltage step is to define the maximum

characteristic time constant (τ_{max}) to measure. In these circumstances all parameters are known, and both C_{LOAD} and R_{LOAD} values can be measured using Equations (2) and (10). Figure 6b depicts the pseudo-code of a routine to implement the measurement of a parallel RC network.

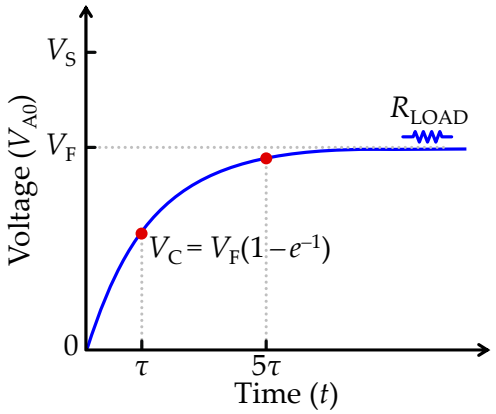

(a)

Pseudo-code:

```
Define highest time constant (τ) to be
measured: tau
Determine time (Δt) until threshold
voltage (V_F): T = 5 × tau
Set port P_A0 and P_A1 to LOW OUTPUT
Wait 1 millisecond: delay (1)
Set port P_A1 to INPUT PULLUP
Wait until Δt = τ : delay (tau)
Sample port P_A1: VC measures V_A1
Wait until Δt = 5τ : delay (T – tau)
Sample port P_A1: VF measures V_A1
R_LOAD is given by Eq.(2) : Replace V_A0 by VF
C_LOAD is given by Eq.(12): Replace V_A1 by VC
                                  t by T
```

(b)

Figure 6. Set-up for recording a load impedance (Z_{LOAD}) formed by a parallel RC network. (**a**) Illustration of the transient response to a voltage step at the input terminal (P_{A0}). (**b**) Pseudo-code used to implement the measurement of a parallel RC network.

2.8. Measurements of an Isolated Load Inductance (L–Meter Mode)

Considering that in the equivalent circuit shown in Figure 1f, Z_{LOAD} is composed of an isolated load inductance (L_{LOAD}), and that for the sake of simplicity, the stray capacitances (C_{pin}) are neglected, which is allowed if they are not larger than some tens of pico-farads (pF), the circuit analysis is simpler than and preferable to using the impedance analysis. Figure 7a shows the impedance representation of the equivalent circuit, where Z_{in} represents the impedance due to the pull-up resistance (R_{pu}) at the input port P_{A1}, and Z_{out} is the output impedance formed by the parallel RC network between the analog input resistance (R_{AIN}) and the series RC network ($Z_{LOAD} + R_{out}$). Z_{LOAD} is the impedance representation of the load inductance (L_{LOAD}), given by $Z_{LOAD} = j\omega L_{LOAD}$. Therefore, an estimation of L_{LOAD} is obtained using the step response of the impedance divider circuit shown in Figure 7a, which is given by:

$$V_{A0}(t) = V_S\left(1 - e^{\frac{-t}{\tau}}\right),\ \tau\ = L_{LOAD}/R_T, \tag{13}$$

where R_T is the total resistance path contributing to the potential difference on the inductance terminals given by $R_T = R_{AIN}\ ||\ R_{pu} + R_{out}$. Thus, L_{LOAD} can be found at any time t by rearranging Equation (13) to:

$$L_{LOAD} = \frac{tR_T}{\ln\left(\frac{V_S}{V_S - V_{A0}(t)}\right)}, \tag{14}$$

where t is the time that takes charges to accumulate in the inductance. Except for the time (t), all parameters in Equation (14) are known and available in Table 1. Therefore, the strategy to solve the time (t) of Equation (14) requires a similar approach, as previously described for the measurement of an isolated capacitance through the transient response. In this case, it must be monitored when the threshold voltage (V_{th}) over L_{LOAD} is approximately

equal to $V_{th} = V_S \cdot (1 - e^{-1})$. As for the isolated capacitance measurement described in Section 2.5.2, the elegant and simpler procedure for testing V_{th}, involves making use of the built-in transistor-transistor logic (TTL) unit to monitor V_{A0} by setting the TTL unit low voltage threshold (V_{IL}) the V_{th} ($V_{th} = V_{IL}$). In practical terms, the elapsed time (Δt) since L_{LOAD} initiates the cycle ($t = 0$) until the TTL unit changes to the logical state low '0' ($V_{A0} \leq V_{IL}$) must be measured, proceeding afterwards to the reading of V_{A0} using the ADC unit (N_{A0}). Then, L_{LOAD} is found by replacing V_{A0} and t with the measured values of N_{A0} and Δt in Equation (14). Figure 7b depicts the voltage step response of the impedance divider circuit. The highlighted region delimited between the voltage level V_{IL} and vs. represents the operation region where the TTL logic unit changes of logic state high '1' to low '0'.

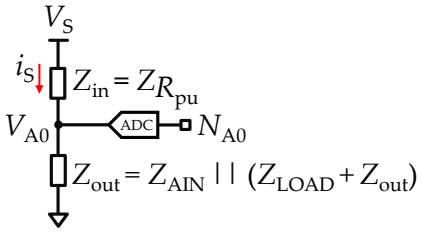

(a)

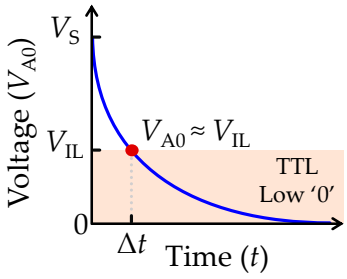

(b)

Pseudo-code:

```
Set port PA0 and PA1 to LOW OUTPUT
Wait 1 millisecond: delay (1)
Set port PA0 to INPUT PULLUP
Read timer: TS measures microseconds
do
  Sample digital port PA0: NA1 measures VA0
while (NA0 == 1)
Read timer: TE measures microseconds
Sample port PA0: NA0 measures VA0
Determine elapsed time (Δt): T = TE - TS
L_LOAD is given by Eq.(14): Replace VA0 by VC
                            t by T
```

(c)

Figure 7. Set-up for recording an isolated load inductance (L_{LOAD}) through the transient acquisition mode. (**a**) Impedance representation of the reduced equivalent circuit. (**b**) Illustration of the step response in voltage measured at the input terminal of L_{LOAD}. V_{IL} is defined in Table 1. (**c**) Pseudo-code used to implement the inductance transient acquisition mode.

The measurement range of the inductance is limited due to the ADC unit resolution, where the technique described above to monitor the transient response to a voltage step is limited by the characteristic time constant (τ) of the circuit, such that if $\tau \to 0$, the charging current velocity (di/dt) of the L_{LOAD} decreases to such proportions that accurately measuring the N_{A0} requires high temporal resolution, since $N_{A0} \to 0$ just before the first reading is taken, causing the ADC unit to overflow. An approximation of the ranging limits of the transient acquisition mode is given by:

$$\frac{\Delta t \cdot R_T}{\ln(N_{max})} \leq L_{LOAD}(t) \leq \frac{\Delta t \cdot R_T}{\ln\left(\frac{N_{max}}{N_{max}-1}\right)} \tag{15}$$

where in Equation (15) the lower and upper resolution of the ADC unit (N_{A0}) are solved assuming $1 \leq N_{A0} \leq N_{max} - 1$. With the same values and assumptions used for the transient C-method, the range of measurement will vary between 0.2 mH $\leq L_{LOAD} \leq$ 1.5 H with R_{pu} = 22.4 kΩ, and 0.4 mH $\leq L_{LOAD} \leq$ 2.7 H with R_{pu} = 41.6 kΩ. These measurable values of L_{LOAD} are not very useful in real life applications, and for that reason in this manuscript only the methodology is provided as proof of concept to perform measurements with AVR® micro-controllers of an isolated inductance. In spite of this, the pseudo-code is

provided in Figure 7c to implement the measurements of an isolated L_{LOAD} through the transient acquisition mode built-in AVR® micro-controllers.

2.9. Data Acquisition and Analysis

The open-source Arduino® IDE software was used to program and upload the scripts on the AVR® micro-controllers. All routines that were programmed to perform the measurements of the RCL-meter are based on the pseudo-codes previously described in each method. The data acquisition was carried out with the serial interface made available on the Arduino® IDE software. The collected data were handled with MATLAB® to perform the data analysis. All measurements were performed at room temperature, about 25 °C.

2.10. Noise and Uncertainty of the Measurements

To achieve the highest measurement accuracy of the RCL parameters, the parasitic capacitances must be minimized by leaving a space of two analog pins between the measured ports, e.g., ports P_{A0} and P_{A3}, and shorten the connection cables to a minimum size.

Additionally, the impact of noise sources in the measurements must be considered. This includes the thermal and $1/f$ contributions, which are not easily modelled, but are included in the global noise measurements. The measured noise of the voltage source (ΔV_n) was 6.7 mV (with the Arduino board powered through the USB interface connected to a local-PC), comparable to the digitalization uncertainty of the ADC (5 mV) described below. This value permits an enhancement of the accuracy of the ADC unit by oversampling techniques. This shows that the digitalization dominates over thermal and $1/f$ noise contributions. Thus, in this analysis we only calculate the effect of digitalization uncertainty. Using the default ADC sampling time of 100 µs, the digitalization uncertainty of a 10-bit ADC unit relative to the reference voltage (V_{REF}) of 5 V, the least significant bit (LSB) voltage is 4.9 mV. To analyze the impact of this digitalization uncertainty, the relative uncertainty (u_r) associated with the analog to digital round off was determined as:

$$u_r = \frac{f(N_{meas}+0.5) - f(N_{meas} - 0.5)}{f(N_{meas})}, \quad (16)$$

where $f(N)$ represents one of the previous Equations (2), (4), (7), (10), (12) and (14) used to determine the R_{LOAD}, C_{LOAD} and L_{LOAD} values. Then, the oversampling technique allow for reducing the digitalization uncertainty (u_r) by a factor of $1/N$ but limited by other sources of uncertainty (noise).

2.11. Relative Accuracy and Precision of the Measurements

The errors associated with the accuracy and precision of the measurements were analyzed through the relative accuracy (a_r) and the relative precision (p_r). The relative precision (p_r) measures the dispersion of the measured impedance values (Z_{meas}) normalized to their average ($\overline{Z}_{meas}$) and was estimated by $p_r = SD(Z_{meas})/\overline{Z}_{meas}$, where SD represents the standard deviation of the measured values. The relative accuracy (a_r) measures the closeness of the measured Z_{meas} to the true or reference value, $Z_{nominal}$, and was estimated by $a_r = |\overline{Z}_{meas} - Z_{nominal}|/Z_{nominal.}$

2.12. Linearization of the ADC Unit

Work was done to improve the linearization of the ADC unit output. By linearization is here meant the maximization of the correlation between measured and nominal values, which depends on the correct knowledge of the micro-controller's parameters. Since all methods presented previously to measure an unknown load impedance (Z_{LOAD}) use the same ports configuration (except for the measurements of an isolated load capacitance using the fast acquisition mode), the simplest method to optimize the linearization of the measurements is to replace Z_{LOAD} with a pure known load resistance (R_{LOAD}) and use different resistor sizes to test and maximize the range and accuracy of the ADC unit. Then, Equation (2) must be used as a fitting function, where the R_{LOAD} values must be

replaced by the nominal values provided by the manufacturer of the resistor, and V_{A0} and vs. by the ADC unit values. Figure 8a shows the N_{A0} values collected with through-hole resistors bridging two ports of the micro-controllers. All samples consist of an average of 100 consecutive measurements. The data were distributed in a logarithmic scale along the horizontal axis according to the nominal resistance value provided by the manufacturer. The red triangles represent the samples measured with the ATmega328P and the blue circles represent the ATmega32U4. Ordinary Least Squares (OLS) were used to fit the data shown in Figure 8a, but with a small twist, which consisted of applying the natural logarithm (ln) to the OLS objective fit function and to the measured N_{A0} values. This proved able to cope better with the large range of resistance values, encompassing several orders of magnitude. Then, to extract the optimized values of R_{AIN}, R_{out} and R_{pu}, the user must provide a guess estimation and use a nonlinear programming solver to find the minimum values of the OLS objective function around the estimated values, taken from the manufacturer datasheets. Table 2 shows the extracted values of R_{AIN}, R_{out} and R_{pu} for both ATmega328P and ATmega32U4 AVR® micro-controllers used in the current work.

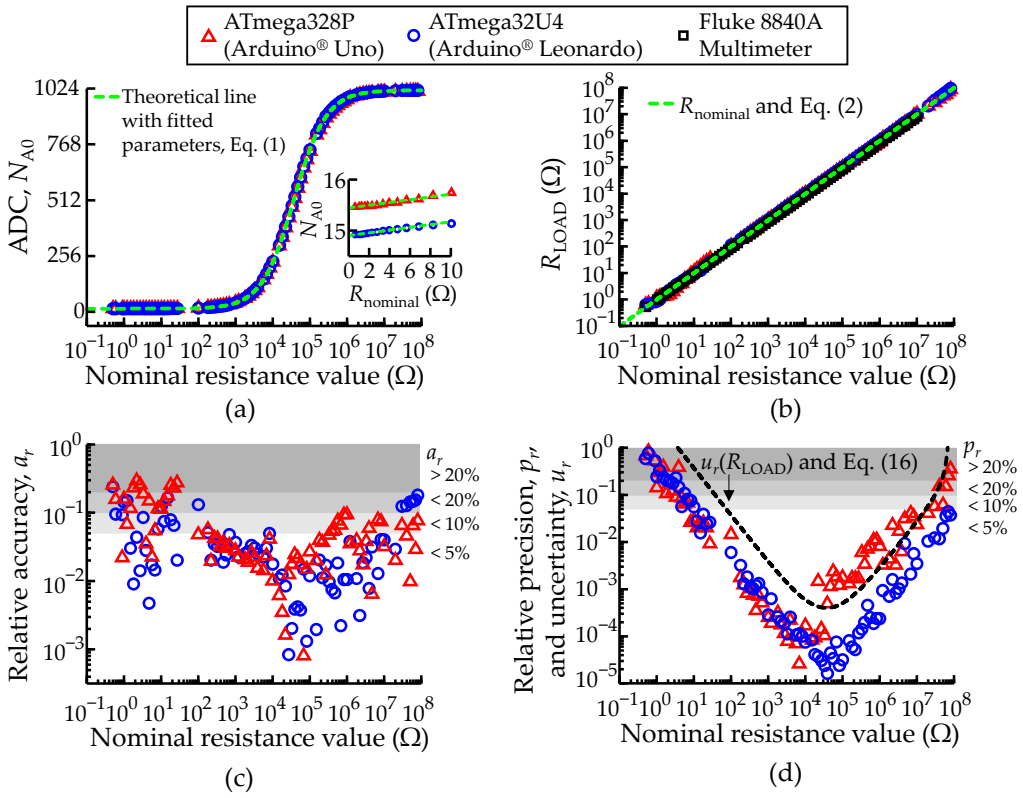

Figure 8. Comparison between the ATmega328P and ATmega32U4 AVR® micro-controllers configured to record an isolated load resistance (R_{LOAD}). (**a**) Measured ADC unit discrete values at port P_{A0} (N_{A0}). Each sample consists of an average of 100 consecutive measurements. (**b**) Measured load resistance (R_{LOAD}) values according to Equation (2). The green dashed lines represent the theoretical lines. (**c**) Relative accuracy (a_r) and (**d**) relative precision (p_r) of the measurements in function of $R_{nominal}$. The black dashed line represents the relative uncertainty (u_r) of the R_{LOAD} measurements according to Equation (16). The white and grey shading areas highlight the levels of u_r, a_r and p_r better than 5%, 10% and 20%. A legend to describe the color scheme used in all plots of Figure 8 was included.

Figure 8a shows the ADC readings as a function of the nominal ADC values. Actual values for both ATmega328P and ATmega32U4 micro-controllers are represented by symbols, and the corresponding fitted lines from Equation (2) (overlapped) in dashed green. The figure inset provides a closer view of the measured samples between 0.5 Ω to 10 Ω. The fitted parameters allow a broad working range of about 8 orders of magnitude for

the measured resistance. Otherwise, using typical values provided by the manufacturer would result in a working range of only 2 orders of magnitude. This procedure was performed only once and the values obtained for R_{AIN}, R_{out} and R_{pu} were used in all the subsequent measurements.

Table 2. Optimized values of the R_{AIN}, R_{out}, R_{pu} and C_{pin} for both ATmega328P and ATmega32U4 AVR® micro-controllers.

ATmega328P				ATmega32U4			
R_{AIN} (MΩ)	R_{pu} (kΩ)	R_{out} (Ω)	C_{pin} (pF)	R_{AIN} (MΩ)	R_{pu} (kΩ)	R_{out} (Ω)	C_{pin} (pF)
3.537	36.89	565.8	23.48	5.451	36.66	542.2	25.5

Likewise, the same fitting analysis previously described was used to optimize the value of C_{pin}, which is required to perform measurements of an isolated load capacitance through the fast acquisition mode. In this case, through-hole capacitors of different sizes were used to bridge two I/O ports of the micro-controller, and Equation (4) was used as a fitting function for the measurements of the N_{A0} values shown in the Figure 9a. The C_{pin} values extracted for each micro-controller are shown in Table 2. The MATLAB scripts written to perform the OLS fitting are available in the Supplementary Materials.

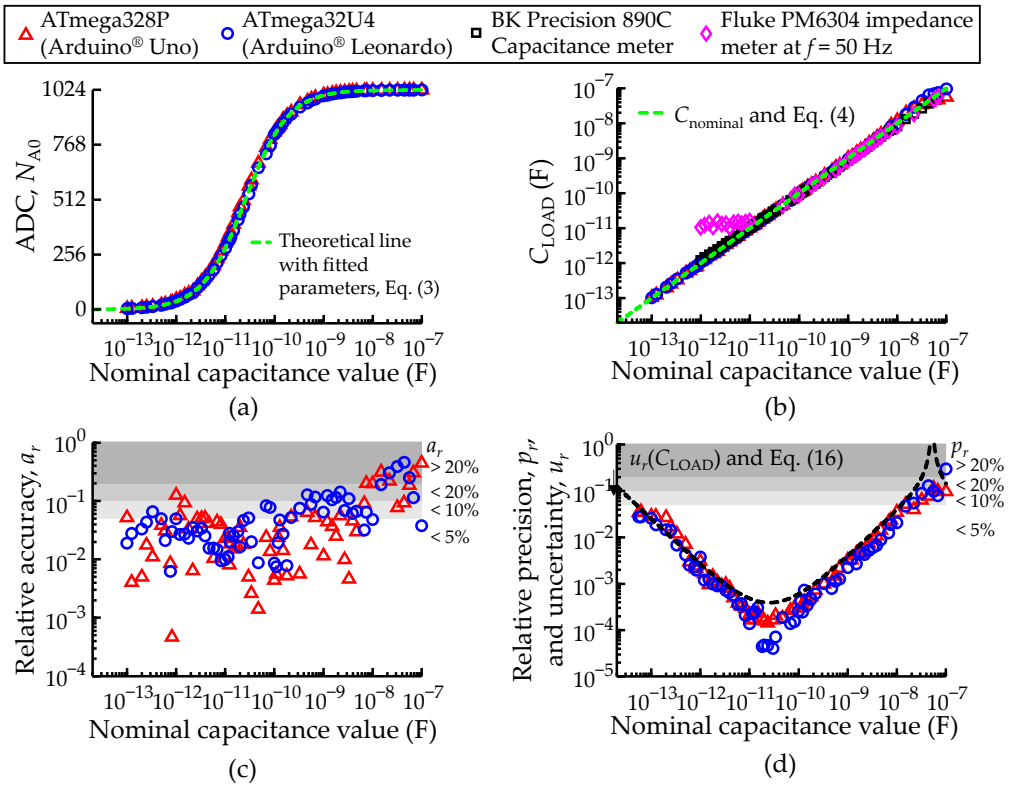

Figure 9. Comparison between the ATmega328P and ATmega32U4 AVR® micro-controllers configured to record an isolated load capacitance (C_{LOAD}) through the fast acquisition mode. (**a**) Measured ADC values at port P_{A0} (N_{A0}). Each ADC sample consists of an average of 100 consecutive measurements. (**b**) Measured load capacitance (C_{LOAD}) given by Equation (4). The green dashed lines represent the theoretical lines. (**c**) Relative accuracy (a_r) and (**d**) relative precision (p_r) of the measurements in function of $C_{nominal}$. The black dashed line represents the relative uncertainty (u_r) of the C_{LOAD} measurements according to Equation (16). The white and grey shading areas highlight the levels of u_r, a_r and p_r better than 5%, 10% and 20%. A legend to describe the color scheme used in all plots of Figure 9 was included.

3. Results

Commercial through-hole resistors and capacitors in the ranges 0.5 Ω–80 MΩ and 100 Ff–4.7 mF (±5%), respectively, were used to perform measurements of either isolated or in series and parallel electrical components with the AVR® micro-controllers. The capacitances in the fF range were of SMD type (Kyocera AVX, Fountain Inn, SC, USA), and all capacitances above 1 µF were aluminum electrolyte capacitor type. The validations were made by comparing the measurements results with the components' nominal values. In all cases, each data point corresponds to the average of 100 measurements performed in a continuous loop.

3.1. Characterization of Isolated Resistance Measurements

The resistance measurements were performed with a set of resistors independent of those used to linearize the ADC. Using the methodology described in Section 2.4, the voltages at port P_{A0} (V_{A0}) were recorded with the ADC unit (N_{A0}), and the measurements were inserted in Equation (2), to obtain the R_{LOAD} values shown in Figure 8b. This figure also includes the same resistances measurements recorded with a commercial instrument, the Fluke 8840A multimeter (Fluke Corporation, Everett, WA, USA), for reference and validation. These are excellent results for a low-cost technique. However, it is important to keep in mind that each individual point is the average of 100 consecutive measurements, performed in a loop. Table 3 provides numeric detail on the data shown in Figure 8b.

Table 3. Comparison of the ATmega328P, ATmega32U4 and Fluke 8840A measured load resistance (R_{LOAD}) values ± standard deviation (SD).

$R_{nominal}$	ATmega328P	ATmega32U4	Fluke 8840A		ATmega328P	ATmega32U4	Fluke 8840A
	R_{LOAD} ± SD			$R_{nominal}$	R_{LOAD} ± SD		
0.5 Ω	0.6 ± 0.4	0.62 ± 0.4	0.548 ± 0.001	5.6 kΩ	5.679 ± 0.001	5.7261 ± 0.0006	5.5390 ± 0.0002
1 Ω	1.2 ± 0.2	0.86 ± 0.2	1.044 ± 0.001	8.2 kΩ	8.539 ± 0.009	8.6078 ± 0.0009	8.1837 ± 0.0002
2.2 Ω	1.6 ± 0.3	2.30 ± 0.5	2.247 ± 0.001	10 kΩ	10.101 ± 0.002	10.1772 ± 0.0008	9.9313 ± 0.0002
5.6 Ω	5.7 ± 0.4	5.70 ± 0.6	5.645 ± 0.001	22 kΩ	21.9 ± 0.3	22.1858 ± 0.0008	21.846 ± 0.0000
8.2 Ω	9.1 ± 0.2	7.72 ± 0.6	8.251 ± 0.001	56 kΩ	55.0 ± 0.1	55.789 ± 0.002	55.8529 ± 0.0003
10 Ω	10.5 ± 0.3	8.77 ± 0.5	10.031 ± 0.005	82 kΩ	80.8 ± 0.1	81.891 ± 0.002	81.914 ± 0.002
22 Ω	22.4 ± 0.4	20.1 ± 0.5	21.901 ± 0.002	100 kΩ	97.3 ± 0.2	98.812 ± 0.003	98.622 ± 0.008
56 Ω	59.7 ± 0.4	55.7 ± 0.5	56.023 ± 0.004	220 kΩ	211.9 ± 0.4	217.55 ± 0.01	219.267 ± 0.007
82 Ω	83.3 ± 0.3	83.1 ± 0.4	82.532 ± 0.0014	560 kΩ	535 ± 5	549.7 ± 0.1	561.045 ± 0.009
100 Ω	102.2 ± 0.3	101.9 ± 0.4	99.44 ± 0.02	820 kΩ	777 ± 7	811.4 ± 0.2	824.71 ± 0.01
220 Ω	224.3 ± 0.3	224.2 ± 0.4	220.560 ± 0.004	1 MΩ	0.906 ± 0.007	0.9894 ± 0.0002	1.0140 ± 0.00004
560 Ω	576.9 ± 0.4	573.6 ± 0.8	556.14 ± 0.01	2.2 MΩ	2.14 ± 0.05	2.193 ± 0.004	2.2171 ± 0.0002
820 Ω	835.8 ± 0.6	833.840 ± 0.0001	817.19 ± 0.03	6.8 MΩ	6.3 ± 0.3	6.89 ± 0.01	6.986 ± 0.002
1 kΩ	1.0348 ± 0.0006	1.0331 ± 0.0004	0.9945 ± 0.0001	8.2 MΩ	8.8 ± 0.3	7.87 ± 0.05	8.2066 ± 0.0001
2.2 kΩ	2.242 ± 0.001	2.2596 ± 0.0005	2.1955 ± 0.0001	10 MΩ	10.3 ± 0.2	9.60 ± 0.03	10.129 ± 0.008

Figure 8c shows the relative accuracy (a_r) of the measurements as a function of the nominal resistance, as defined in Section 2.11. Figure 8d shows their relative precision, p_r, also defined in Section 2.11 (data points), and the estimated upper limit for the relative uncertainty caused by the digitalization round-off error, u_r, defined in Equation (16) and represented by the dashed line. Note that the standard deviations are calculated on samples that are already averages of 100 points, which means that u_r should be divided by 10, for a correct comparison with p_r. Both plots include white and grey shading regions to highlight the levels of a_r and p_r better than 5%, 10% and 20%. The two plots show better

performance of the method in the intermediate resistance range and its degradation in the regime of very low or very high resistances. This is because the lower and upper limits for R_{LOAD} correspond to N_{A0} tending to the higher (N_{max}) and lower ($\approx$0) values of the digital output, respectively, where the roundoff errors introduced by digitalization become more important, affecting both precision and accuracy.

Most of the data points lay below the u_r curve. This is because u_r is merely an upper limit for the digitalization noise, which is actually lower. In any case, the plot indicates that the main uncertainty source in the determination of resistance is the digitalization roundoff.

In terms of performance, the ATmega32U4 delivers better results. The range defined by $p_r < 5\%$ is approximately 10 Ω–10 MΩ for the ATmega328P and 10 Ω–80 MΩ for the ATmega32U4, while the range defined by $a_r < 5\%$ is 100 Ω–100 kΩ for the ATmega328P and 100 Ω–10 MΩ for the ATmega32U4.

The sensitivity of the R-meter (minimum detectable increment in resistance) was assessed at a representative value of 1 kΩ, as well at increments of 0.5, 1 and 4.7 Ω. 50 measurements were acquired at each resistance value. The average of the 50 ADC counts were plotted against the resistance values and a local slope ADC counts/Ω was determined. The standard deviations of the 4 measurements were also calculated and averaged to get a typical value. A conservative estimative of the sensitivity was then performed by calculating the increase in resistance needed to shift the ADC count by two standard deviations, which was about 1.2 Ω or 0.1% of the nominal value. Additionally, a student *t*-test analysis was performed by comparing all the 4 datasets of 50 measurements against each other to conclude that they were all different ($p < 0.05$). This suggested that even an increment of 0.5 Ω is enough to change the output of the R-meter, which is about 2 times less than the previous conservative estimate.

3.2. Characterization of Isolated Capacitance Measurements: Fast Acquisition Method

Using the methodology described in Section 2.5.1 with different commercial capacitors varying from 100 fF to 100 nF, measurements of the voltage at port P_{A0} (V_{A0}) were recorded with the ADC unit (N_{A0}) and shown in Figure 9a. Figure 9a also includes a green dashed line that represents the theoretical lines for the two micro-controllers (overlapped), obtained from Equation (3) with the fitted C_{pin} values shown in Table 2. The measured N_{A0} and fitted C_{pin} values were replaced in Equation (4) to determine the load capacitance (C_{LOAD}), shown in Figure 9b. At the end of Section 3.2, Table 4 was included, providing numeric detail on the data shown in Figure 9b. For reference and validation, this plot also includes the measurements recorded with two commercial instruments, the BK Precision 890C capacitance meter (B&K Precision Corporation, Yorba Linda, CA, USA) and the Fluke PM6304 impedance meter (Fluke Corporation, Everett, WA, USA) at the lowest frequency available (f = 50 Hz). The green dashed line is $C_{LOAD} = C_{nominal}$, showing that the C_{LOAD} values determined by both micro-controllers match the target values within the range 100 Ff–10 nF, thus achieving a range of about 5 orders of magnitude.

Figure 9c,d allow a more detailed view of the quality of this match and display a_r, p_r and u_r (in the same way as in Figure 8c,d). The accuracy a_r drops significantly above 10 nF because the voltage drop at the load capacitance tends towards the circuit voltage source ($N_{A0} \rightarrow N_{max}$), as predicted by Equation (5), inducing large errors in the determination of C_{LOAD}.

This is evidenced in the u_r curve represented (black dashed line in Figure 9d), showing the same V-shaped distribution u_r, as described in Figure 8d, for the resistance measurement. The overlap between u_r and p_r means that the main source of variability is the digitalization noise, to which the fast C-meter adds almost no contribution.

Table 4. Comparison of the ATmega328P, ATmega32U4 and Fluke 8840A measured load capacitance (C_{LOAD}) values ± standard deviation (SD) through the fast acquisition mode.

$C_{nominal}$	ATmega-328P	ATmega-32U4	Fluke PM6304	BK 890C		ATmega-328P	ATmega-32U4	Fluke PM6304	BK 890C
	C_{LOAD} ± SD				$C_{nominal}$	C_{LOAD} ± SD			
1 pF	1.126 ± 0.004	1.050 ± 0.005	12 ± 8	1.3 ± 0.6	560 pF	550.0 ± 0.8	510.89 ± 0.05	526 ± 3	531 ± 3
1.5 pF	1.640 ± 0.002	1.541 ± 0.003	16 ± 18	1.9 ± 0.3	680 pF	644 ± 1	600.30 ± 0.05	678 ± 5	677 ± 7
2.7 pF	2.834 ± 0.003	2.782 ± 0.004	14 ± 8	3.3 ± 0.6	1 nF	1.012 ± 0.003	0.93558 ± 0.00004	0.999 ± 0.009	1.008 ± 0.004
3.9 pF	4.101 ± 0.003	3.998 ± 0.004	12 ± 5	8 ± 1	1.5 nF	1.445 ± 0.007	1.34302 ± 0.00003	1.493 ± 0.005	1.517 ± 0.002
5.8 pF	5.860 ± 0.002	5.709 ± 0.003	17 ± 19	7 ± 3	2.2 nF	2.08 ± 0.01	1.88744 ± 0.00004	2.185 ± 0.005	2.24 ± 0.01
8.2 pF	8.527 ± 0.003	8.278 ± 0.003	17 ± 5	9.3 ± 0.4	3.3 nF	3.29 ± 0.03	2.93701 ± 0.00003	3.314 ± 0.006	3.401 ± 0.003
10 pF	10.231 ± 0.002	9.900 ± 0.002	18 ± 5	11.2 ± 0.3	6.8 nF	7.4 ± 0.2	6.58318 ± 0.00003	7.096 ± 0.02	7.13 ± 0.06
20 pF	20.711 ± 0.003	19.672 ± 0.002	25 ± 4	22.300 ± 0.000	7.5 nF	9.0 ± 0.2	7.98201 ± 0.00004	7.56 ± 0.05	7.7540 ± 0.0004
47 pF	46.934 ± 0.009	46.59 ± 0.04	49 ± 7	49.3 ± 0.5	10 nF	12.0 ± 0.4	9.51585 ± 0.00003	10.15 ± 0.07	9.668 ± 0.001
82 pF	80.88 ± 0.02	81.01 ± 0.02	89 ± 7	83.4 ± 0.5	15 nF	20 ± 1	17.8541 ± 0.00004	15.44 ± 0.06	15.570 ± 0.0000
100 pF	99.56 ± 0.04	100.87 ± 0.03	99 ± 5	103.183 ± 0.04	22 nF	27 ± 1	28.6855 ± 0.00003	21.623 ± 0.007	22 ± 1
180 pF	179.1 ± 0.1	178.6 ± 0.2	187 ± 1	185 ± 1	56 nF	46 ± 5	70.0663 ± 0.00002	57.21 ± 0.04	57.2 ± 0.9
220 pF	210.7 ± 0.2	208.5 ± 0.2	221 ± 12	217.6 ± 0.5	68 nF	47 ± 5	75.7749 ± 0.00002	68.39 ± 0.07	69 ± 2
470 pF	440.0 ± 0.7	409.77 ± 0.05	469 ± 6	449.9 ± 0.8	100 nF	55 ± 5	96.2257 ± 0.00003	101.3 ± 0.02	101.536 ± 0.005

The sensitivity estimates were performed according to the same lines described in Section 3.1, this time for the representative values of 18 pF and 22 pF, with small increments of 1, 1.2 and 1.5 pF. The sensitivity was estimated to be about 10–20 fF in both cases. The student *t*-test analysis also concluded that all the capacitance measurement datasets were different from each other ($p < 0.05$).

3.3. Characterization of Isolated Capacitance Measurements: Transient Acquisition Method

The capacitance meter in the transient mode was tested according to the methodology described in Section 2.5.2 with different commercial capacitors ranging from 100 pF to 4.7 mF. The transient acquisition mode requires waiting until the TTL logic unit returns '1' and the elapsed time (Δt) until that transition. The measurements of port P_{A0} (N_{A0}), taken at the transition and the corresponding elapsed time (Δt) are shown in Figure 10a.

The upper graph shows N_{A0} as symbols. Note that by definition these N_{A0} readings correspond to TTL parameter V_{IH}—High-Level Input Voltage (because they are acquired at the transition). The same graph shows that the lower the capacitance, the higher the V_{IH} of the TTL unit. This aspect is consistent with the expected operation mode of the TTL unit. In fact, the TTL unit uses the output high-level current (i_{HL}) as a test condition, thence, as $C_{LOAD} \rightarrow C_{pin}$, the more leakage current flows through C_{LOAD}, leading to a non-constant V_{IH}. It should be remarked that the inconstancy of the threshold does not represent a problem for the application of Equation (7), since it only requires a given time and the associated reading V_{A0}.

V_{IH} stabilizes above 22 nF because in that range i_{HL} remains essentially undisturbed. This allows the estimation of the "basal" V_{IH} (ΔN_{A0}) averaging the values of N_{A0} at the transition for all samples above 22 nF, specifically $\Delta N_{A0} \cong 536$ for the ATmega328P and $\Delta N_{A0} \cong 331$ for the ATmega32U4, which are represented by the green dashed lines. The measured values of ΔN_{A0} are consistent with the typical values described in Table 1.

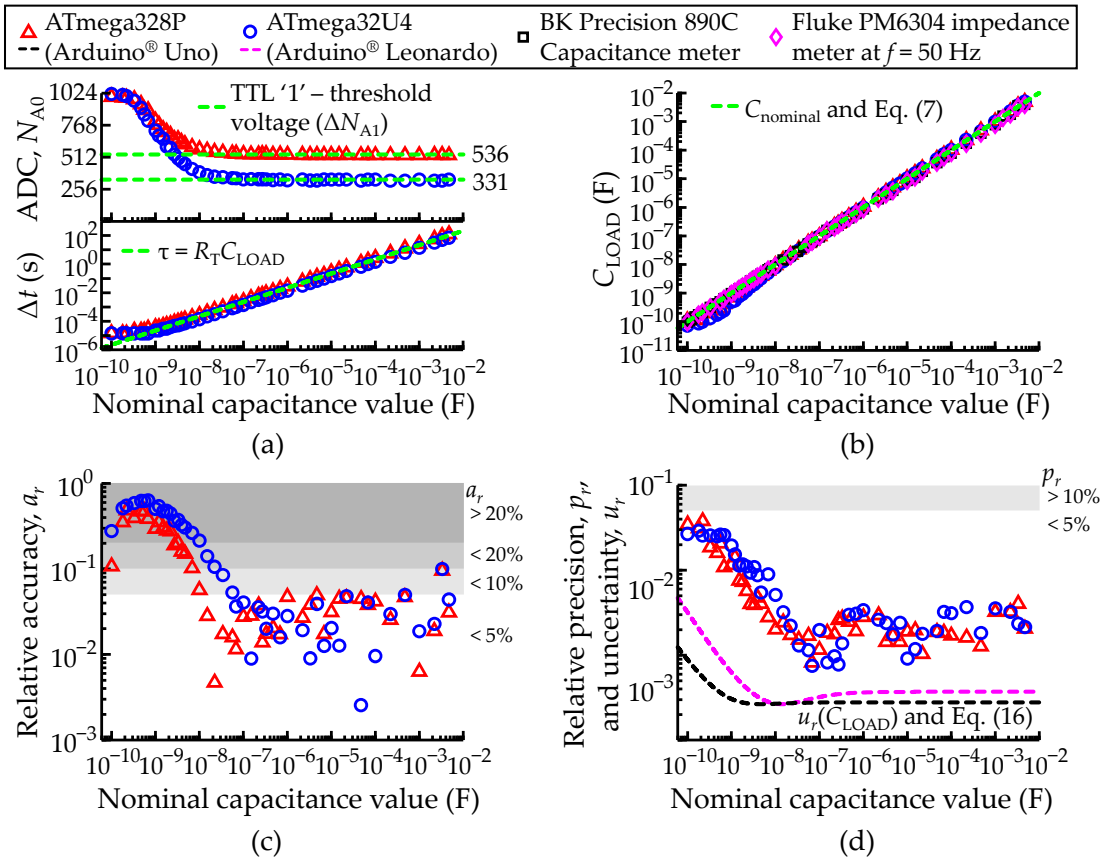

Figure 10. Comparison between the ATmega328P and ATmega32U4 AVR® micro-controllers configured to record an isolated load capacitance (C_{LOAD}) through the transient acquisition mode. (**a**) Measured ADC value and time (Δt) until the TTL unit changes to digital state high, logic '1' at port P_{A0} (N_{A0}). Each ADC and Δt sample consist of an average of 100 consecutive measurements. (**b**) Measured load capacitance (C_{LOAD}) given by Equation (7). The green dashed lines represent the theoretical lines. (**c**) Relative accuracy (a_r) and (**d**) relative precision (p_r) of the measurements in function of $C_{nominal}$. The black dashed line represents the relative uncertainty (u_r) of the C_{LOAD} measurements according to Equation (16). The white and grey shading areas highlight the levels of u_r, a_r and p_r better than 5%, 10% and 20%. A legend to describe the color scheme used in all plots of Figure 10 was included.

The measured elapsed time (Δt) shown in the bottom graph of Figure 10a closely matches the green dashed line, which represents the characteristic time constant $\tau = R_T C_{LOAD}$, where $R_T = R_{AIN} \,||\, R_{pu} + R_{out}$. The linearity still holds in spite of a non-constant V_{IH} due to the role of i_{HL}, since the leakage current is also determined by the RC constant of the circuit. The RT values differ only slightly for the two micro-controllers ($R_T \cong 35$ kΩ for ATmega328P and $R_T \cong 37$ kΩ for ATmega32U4), causing overlap of the corresponding time constant lines.

For the smallest capacitances ($C_{LOAD} < 1$ nF), Δt tends toward a plateau (Δt_{min}) given by 12.5 µs for both micro-controllers, because $C_{LOAD} \rightarrow C_{pin}$. Thus, the C_{LOAD} values determined with Equation (7), and shown in Figure 10b, are affected by larger errors in the low capacitance range. This is not very apparent in this figure, where the data points seem very close to the green dashed line ($C_{LOAD} = C_{nominal}$) because of the logarithmic scale. Still, at the end of Section 3.3, Table 5 provides numeric detail on the data shown in Figure 10b.

Table 5. Comparison of the ATmega328P, ATmega32U4 and Fluke 8840A measured load capacitance (C_{LOAD}) values ± standard deviation (SD) through the transient acquisition mode.

$C_{nominal}$	ATmega-328P	ATmega-32U4	Fluke PM6304	BK 890C		ATmega-328P	ATmega-32U4	Fluke PM6304	BK 890C
	C_{LOAD} ± SD				$C_{nominal}$	C_{LOAD} ± SD			
100 pF	111 ± 4	72 ± 1	99 ± 5	101.41 ± 0.04	2.2 µF	2.259 ± 0.007	2.158 ± 0.006	2.2742 ± 0.0004	2.292 ± 0.005
1 nF	0.703 ± 0.008	0.49 ± 0.01	0.999 ± 0.009	1.008 ± 0.004	4.7 µF	4.933 ± 0.008	4.883 ± 0.009	4.24 ± 0.04	4.5010 ± 0.0006
2.2 nF	1.591 ± 0.009	1.22 ± 0.01	2.185 ± 0.005	2.24 ± 0.01	6.8 µF	6.92 ± 0.01	6.71 ± 0.02	7.1687 ± 0.0001	7.1870 ± 0.0001
4.7 nF	3.99 ± 0.02	3.26 ± 0.02	4.77 ± 0.03	4.90 ± 0.03	10 µF	10.31 ± 0.02	10.204 ± 0.009	9.76 ± 0.01	9.998 ± 0.02
6.8 nF	6.10 ± 0.02	5.01 ± 0.05	7.10 ± 0.02	7.13 ± 0.06	22 µF	23.01 ± 0.02	23.06 ± 0.04	20.98 ± 0.03	21.29 ± 0.03
10 nF	9.43 ± 0.02	7.85 ± 0.04	10.15 ± 0.07	9.667 ± 0.001	47 µF	49.10 ± 0.09	47.12 ± 0.09	42.69 ± 0.04	43.0 ± 0.5
22 nF	22.10 ± 0.04	19.66 ± 0.04	21.623 ± 0.007	22 ± 1	68 µF	70.6 ± 0.1	70.8 ± 0.2	66.39 ± 0.02	68.68 ± 0.06
56 nF	56.89 ± 0.09	53.03 ± 0.06	57.21 ± 0.04	57.2 ± 0.9	100 µF	104.2 ± 0.2	101.0 ± 0.3	98.14 ± 0.04	102.30 ± 0.08
68 nF	67.22 ± 0.06	65.52 ± 0.05	68.39 ± 0.07	69 ± 2	220 µF	225.6 ± 0.4	226.5 ± 0.8	200.29 ± 0.08	206.7 ± 2
100 nF	97.2 ± 0.1	95.9 ± 0.2	101.34 ± 0.02	101.536 ± 0.005	470 µF	491.9 ± 0.6	446.6 ± 0.8	455.7 ± 0.2	472.6 ± 3
220 nF	228.3 ± 0.4	212.2 ± 0.2	221.79 ± 0.03	221.900 ± 0.000	1 mF	1.006 ± 0.003	0.981 ± 0.004	0.9608 ± 0.0006	0.994 ± 0.006
470 nF	480 ± 1	456 ± 1	468.54 ± 0.05	469.800 ± 0.000	2.2 mF	2.240 ± 0.007	2.250 ± 0.007	2.1667 ± 0.0005	2.1987 ± 0.0000
680 nF	692 ± 1	669 ± 2	665.67 ± 0.2	680.000 ± 0.000	3.3 mF	3.62 ± 0.02	3.631 ± 0.009	3.1891 ± 0.0007	3.441 ± 0.002
1 µF	1.047 ± 0.003	0.972 ± 0.003	0.983 ± 0.001	0.989 ± 0.007	4.7 mF	4.85 ± 0.01	4.91 ± 0.01	4.6754 ± 0.0005	4.935 ± 0.003

The plots of a_r in Figure 10c illustrate better the difficulties in the low capacitance ranges. The relative accuracy drops significantly (worse than 5%) below 70 nF for the ATmega32U4 and below 10 nF for the ATmega328P. However, both remain, at least, on a 5% accuracy level above those critical values, representing a linear response of the instrument across 6 decades.

Figure 10d shows p_r (points) and u_r (dashed lines). Contrary to the fast C-meter case, here the u_r and p_r lines are clearly above u_r, which means that the method introduces sources of noise other than digitalization. This is probably because variations of some ADC units in the threshold level impact much more the measurement than one ADC unit only, related to the digitalization error. These variations may be caused by the internal noise of the micro-processors. The performance degradation in the low capacitance regime is also evident from this figure.

The sensitivity estimates were performed according to the same lines described in Section 3.1, for the representative value of 1 µF, with small increments of 1.8, 2.2, 2.7, 3.3, 3.9 and 4.7 nF. The sensitivity was estimated to be about 10–20 fF in both cases. The student *t*-test analysis also concluded that all the capacitance measurement datasets were different from each other ($p < 0.05$).

3.4. Characterization of Measurements for Serial RC Networks

Using different sets of commercial resistors varying in factors of 10, from 10 Ω to 10 MΩ, and capacitors with 2 samples per order of magnitude, from 100 pF to 4.7 mF, seven trials were made to test the methodology described in Section 2.6. Each trial consisted of keeping the R_{LOAD} constant and varying the C_{LOAD}. Figure 11 compiles a total of 14 trials carried out with the two micro-controllers. The white points with red edges represent the data measured with the ATmega328P, and the blue points represent the ATmega32U4. They are mostly overlapped.

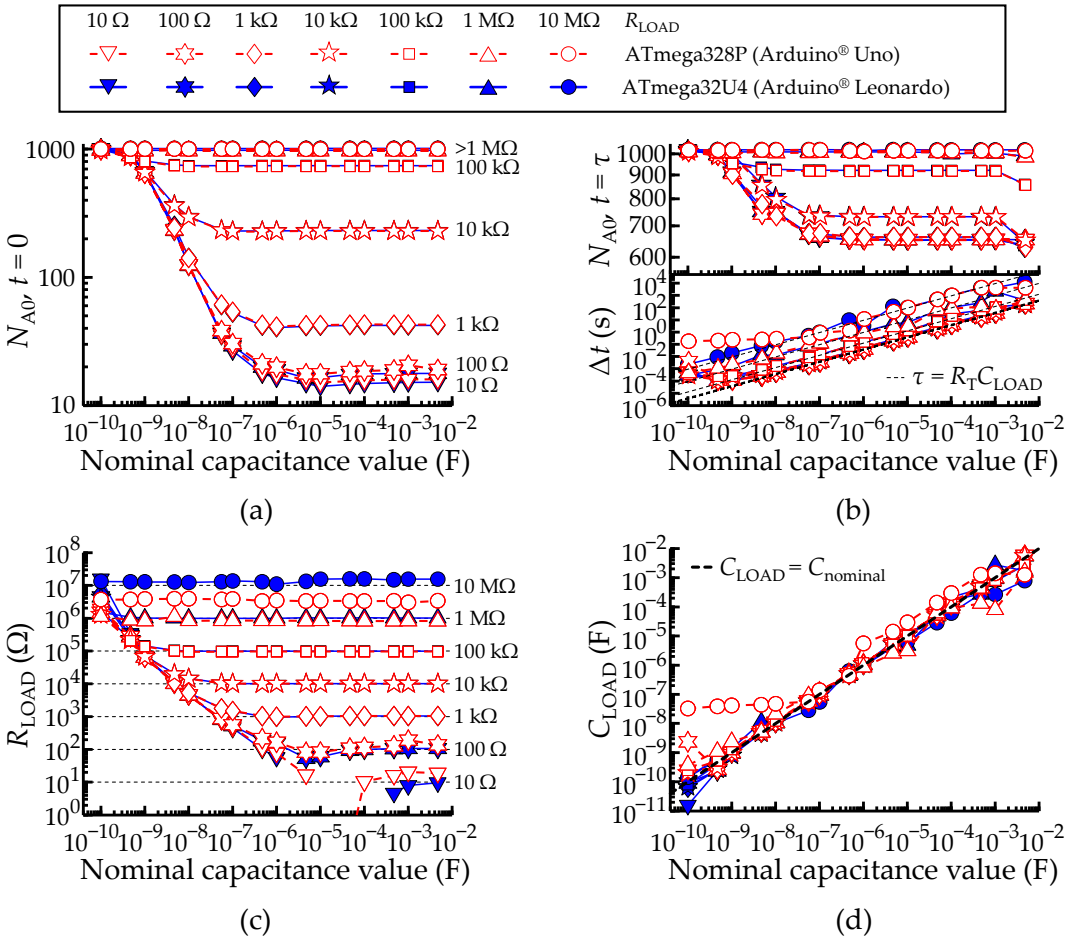

Figure 11. Comparison between the ATmega328P and ATmega32U4 AVR® micro-controllers configured to measure a serial RC network. (**a**) Measured ADC value at $t = 0$. (**b**) Measured ADC value and time (Δt) until $V_{A1} \geq V_C$. (**c**,**d**) Obtained R_{LOAD} and C_{LOAD} values according to Equations (2) and (10), respectively. A legend to describe the color scheme used in all plots of Figure 11 was included. The black dashed lines always represent the theoretical lines.

The method implies measurement of the port P_{A0} voltage level (V_{A0}) at $t = 0$ to find the offset voltage (V_R) and at $t = \Delta t \geq \tau$, to find the voltage level V_C (defined in Section 2.6).

Figure 11a,b show the measured discrete values (N_{A0}) at the instants $t = 0$ and $t \geq \tau$, respectively, with both micro-controllers. Figure 11b also includes in the bottom graph the measured elapsed time (Δt) until $V_{A1} \geq V_C$, together with the theoretical time constants, $\tau = R_T C_{LOAD}$. Note that, from Equation (9), $N_{A0}(t = 0) = V_R$, which is independent of C_{LOAD}. This means that all the curves in Figure 11a should be horizontal lines. However, the minimum available acquisition time (ca. 3 µs) is insufficient to capture the initial curve values for $C_{LOAD} < 1$ µF. Thus, the captured N_{A0} values at $t = 0$ tend to N_{max} in the limit of very small capacitances. This explains why the (ideal) straight lines become distorted in Figure 11a, especially for lower R_{LOAD}. Likewise, the plateau N_{A0} ($t \geq \tau$) = V_C is reached for any $C_{LOAD} > 100$ nF, which hampers the measurements of N_{A0} after $t \geq \tau$ in this range and induces the same type of distortion in Figure 11b, top.

R_{LOAD} and C_{LOAD} were determined through the use of Equations (2) and (10), with the results shown in Figure 11c,d, respectively. The horizontal lines in Figure 11c represent the ideal result, $R_{measured} = R_{LOAD}$. The measured R_{LOAD} values are unreliable within a domain in the R-C plane approximately defined by $R_{nominal}\, C_{nominal} < 10^{-4}$ s.

As discussed above, the system loses accuracy for smaller values of R_{LOAD}. In fact, when $R_{LOAD} \ll (R_{AIN} \,||\, R_{pu}) + R_{out}$, then $R_T = (R_{AIN} \,||\, R_{pu}) + R_{LOAD} + R_{out} \approx R_{pu} + R_{out}$, and the information about R_{LOAD} is lost. For this reason, the higher the R_{LOAD}, the better

the accuracy. This observation is valid for both micro-controllers, except for the trials performed with a R_{LOAD} of 10 MΩ since $N_{A0} \rightarrow N_{max}$ at $t = 0$.

The measurements of the elapsed time (Δt), after $V_{A0} \geq V_C$, shown in the bottom graph of Figure 11b, exhibit a relative shift in the vertical axis due to the different R_{LOAD} values. Deviations from the straight line are consequence of the excess digitalization uncertainty. This aspect is evidenced after determination of the C_{LOAD} values using Equation (10) and shown in Figure 11d, where the deviations from the black dashed line ($C_{LOAD} = C_{nominal}$) relate to the excess digitalization uncertainty.

Overall, there is a trade-off between the R_{LOAD} and C_{LOAD} ranges for best accuracy. There are three extreme regimes: (case 1) R_{LOAD} is large (>1 MΩ), irrespective of the C_{LOAD} value: the accuracy of the measurements is good for the resistance and poor for the capacitance; (case 2) small R_{LOAD} (<100 kΩ) and large C_{LOAD} (>1 nF): measurements with poor accuracy for the resistance, good for the capacitance; (case 3) small R_{LOAD} (<100 kΩ) and small C_{LOAD} (<0.1 nF): measurements with very poor accuracy for the resistance, poor for the capacitance. Outside these extreme regimes, the accuracy is at least acceptable for R_{LOAD} and C_{LOAD} simultaneously.

3.5. Characterization of Measurements for Parallel RC Networks

The experimental procedures to perform the characterization of measurements for parallel RC networks were the same as those of the previous section.

For the parallel RC, the saturation voltage (V_F) lies below V_S, and it is necessary to determine both V_F and τ from the data. There are simple and computationally light algorithms allowing the identification of a stationary plateau, such as that occurring at V_F. These have been tested and verified, but including here the description of such methods would increase the length of this report. Thus, the subsequent analysis assumes that τ is already known. No generality is lost with this assumption.

Therefore, to each combination of a parallel RC network (R_{LOAD} || C_{LOAD}) that was measured, the time constant τ was directly assumed as $R_T C_{LOAD}$. The total acquisition time was set to 10τ, V_F was read from V_{A0} at $t = 5\tau$ and V_C was read from V_{A0} at $t = \tau$.

Figure 12 aligns the results in two columns. The left column [(a) and (c)] refers to the measurements of R_{LOAD} values and the right one [(b) and (d)] refers to the measurements of C_{LOAD} values. The N_{A0} values at the instants $t = 5\tau$ and $t = \tau$ are shown in Figure 12a,b, respectively. Figure 12c,d show the R_{LOAD} and C_{LOAD} values, which were obtained from Equations (2) and (12), respectively.

The R_{LOAD} values are generally in line with the measurements carried on with isolated resistors shown in Figure 8b, but with few deviations to linearity (at 10 Ω and any C_{LOAD}, for the ATmega328P; at 1 MΩ and C_{LOAD} > 1 μF, for both micro-controllers).

As discussed before, in Section 3.4, a too large minimal acquisition time and/or the excess of digitalization noise are the reason the collected samples deviate from the theoretical lines represented by the horizontal black dashed lines. Similarly, the C_{LOAD} values are in line with the measurements carried on with isolated capacitors shown in Figure 9b. However, the accuracy of the measurements is variable, for the same reasons mentioned above.

Overall, there is a trade-off between the R_{LOAD} and C_{LOAD} ranges for best accuracy. There are two extreme regimes: (case 1) C_{LOAD} is small (<1 μF), and R_{LOAD} is large (<1 kΩ): the accuracy of the measurements is good for the resistance and poor for the capacitance; (case 2) large R_{LOAD} (>1 MΩ) and small C_{LOAD} (<1 μF): measurements with very poor accuracy for the capacitance, and poor for the resistance. Outside these extreme regimes, the accuracy is at least acceptable for R_{LOAD} and C_{LOAD} simultaneously.

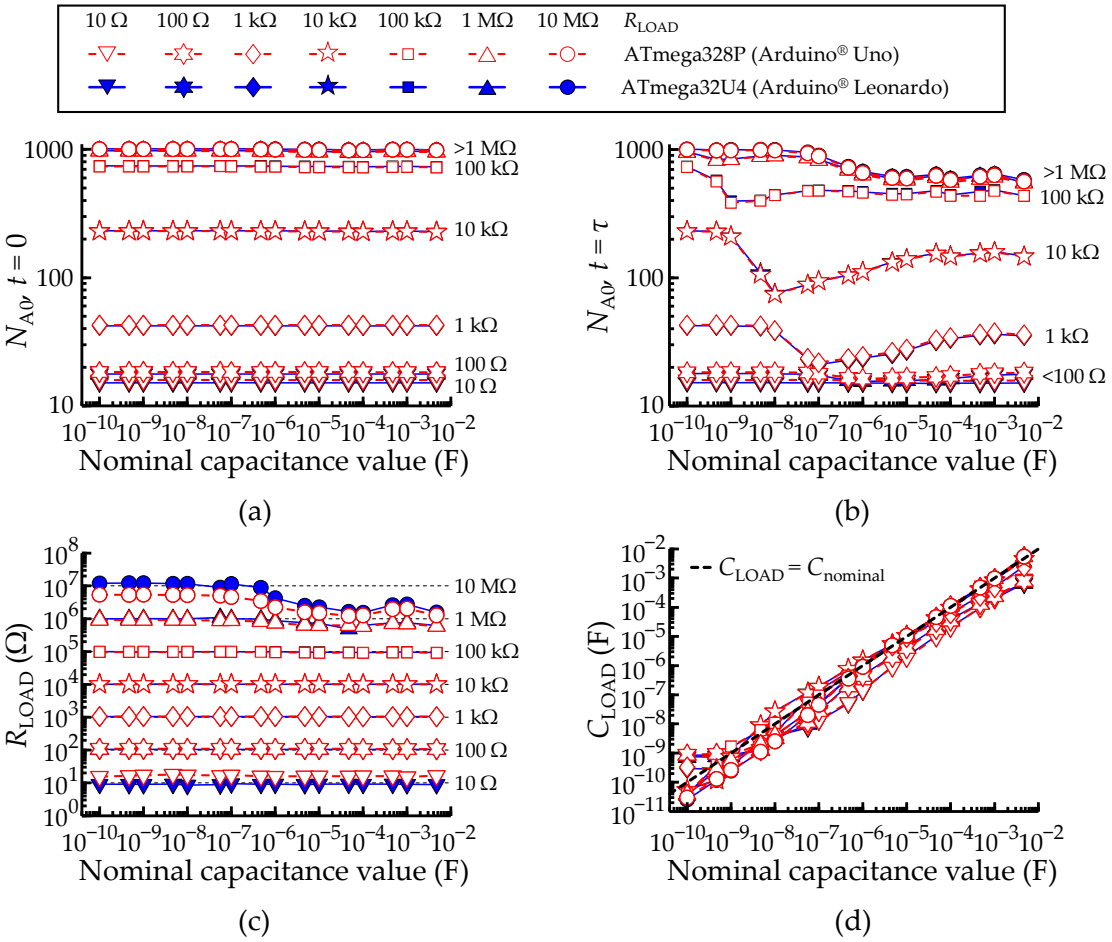

Figure 12. Comparison between the ATmega328P and ATmega32U4 AVR® micro-controllers configured to measure a parallel RC network. (**a**) Measured ADC value at $t = 5\tau$. (**b**) Measured ADC value at $t = \tau$. (**c**,**d**) Obtained R_{LOAD} and C_{LOAD} values according to Equations (2) and (12), respectively. A legend to describe the color scheme used in all plots of Figure 12 was included. The black dashed lines always represent the theoretical lines.

4. Discussion and Conclusions

This work described and characterized methods to accurately measure impedance using Arduino® boards with built-in AVR® micro-controllers. This is highly remarkable considering the ultra-low cost of the hardware. The measurement method allows the extraction of the resistance (R) and capacitance (C) values of either isolated or series and parallel configuration. Furthermore, inductance (L) measurements can be also performed, yet the range of measurable values is not very useful.

To check the cross-platform applicability of our proposed RCL-meter, two different AVR® micro-controllers assembled on Arduino® boards were selected, namely the ATmega328P assembled on an Arduino® Uno and the ATmega32U4 assembled on an Arduino® Leonardo. A benchmark was made to test the performance of micro-processors.

As for the measurements of isolated resistances and capacitances, the ATmega32U4 outperforms the ATmega328P, and some specific differences were identified. For instance, the ATmega32U4 was revealed to be more efficient in terms of acquisition time, providing a significant improvement when recording long-term transients. In the worst-case scenario, when recording an isolated capacitance (C_{LOAD} = 4.7 mF) through the transient acquisition mode, the ATmega32U4 performs two times faster than the ATmega328P. In addition, when measuring both C_{LOAD} and R_{LOAD} values of in-series or parallel RC networks, the ATmega32U4 takes a slight advantage over the ATmega328P for larger values of R_{LOAD}, while, conversely, the ATmega32U4 performs better for larger values of C_{LOAD}.

The noise profiles of the direct measurements (R-meter and fast C-meter) are essentially defined by the digitalization noise, while the transient C-meter brings an important extra noise source from the variability in the determination of instants of time required to perform the calculations.

The fast and transient C-meter methods complement each other, since the fast method is best for low capacitances and the transient method best for high capacitances. Operated together, they are able to deliver a relative accuracy equal to or better than 20% in the range 100 fF–10 mF, that is, across 11 orders of magnitude. Furthermore, the accuracy is equal to or better than 5% in the ranges 100 fF–100 pF and 100 nF–10 mF. The series and parallel RC combinations are also able to deliver good measurements of R and C in specific domains of the R-C plane.

Additional investigations were made to analyze the performance of both Arduino® boards supplied via a large power bank (Litionite Tanker 90 W/50,000 mAh) and using a data logger shield (RobotDyn™, Zhuhai, China) to store the measurements in a local micro-SD card. This work led to the conclusion that no substantial improvements are achieved by using a low-noise and low-uncertainty voltage supply, and therefore all presented data considers the typical noise and uncertainty from a common USB interface voltage supply source. However, the voltage supply unit determines the overall measurement quality in regions close to the ADC unit threshold values (N) for $N < 20$ or $N > 1000$.

Additionally, measurements of the same R_{LOAD} and C_{LOAD} values were made with commercial instruments and presented in the manuscript to provide insight on the overall performance of the ATmega328P and ATmega32U4 micro-controllers as a low-cost alternative to more expensive and sophisticated instruments.

Moreover, the concept proposed in this work, based on AVR® micro-controllers, may possibly be extended to other microcontrollers such as the STM32 family based on ARM architecture. The latter have more or improved integrated hardware features relative to the former, such as more flash memory, higher resolution ADC drive and faster clocks. On the other hand, using more sophisticated microcontrollers brings the disadvantage of idle but power-consuming internal hardware, for example, the digital-to-analog unit (DAC), which is not required in the present work. In any case, the inherent specificities of each architecture imply different implementations, difficult to cover in a single report.

The work carried out in the investigation of an ultra-low-cost RCL meter was mainly targeted towards impedimetric biosensor measurements, in order to facilitate the integration of the sensing and processing layers to the IoT. Its simplicity opens new possibilities for the improvement of ongoing and future projects in the field of smart sensing. The long-term goal of this work is to integrate the control of the sensing and processing layers into the Web of Things (WoT), which is an upper layer of interaction between devices that may be managed by artificial intelligence.

Supplementary Materials: The following supporting information can be downloaded at: https://www.mdpi.com/article/10.3390/s22062227/s1, C++ code A.1: High-level routine to measure isolated resistances; C++ code A.2: High-level routine to measure isolated capacitances through the fast acquisition mode; C++ code A.3: High-level routine to measure isolated capacitances through the transient acquisition mode; C++ code A.4: High-level routine to measure a series RC-network; C++ code A.5: High-level routine to measure a parallel RC-network; C++ code A.6: High-level routine to measure an isolated inductance; MATLAB code B.1: High-level routine for fitting the Ordinary Least Squares (OLS) function to the resistance values; MATLAB code B.2: High-level routine for fitting the Ordinary Least Squares (OLS) function to the capacitance values.

Author Contributions: Conceptualization, P.M.C.I. and P.S.; methodology, P.M.C.I. and P.S.; software, P.M.C.I.; validation, P.M.C.I.; formal analysis, P.M.C.I.; investigation, P.M.C.I. and R.G.; resources, R.G.; data curation, P.M.C.I.; writing—original draft preparation, P.M.C.I.; writing—review and editing, R.G. and P.S.; supervision, P.S.; project administration, R.G.; funding acquisition, R.G. All authors have read and agreed to the published version of the manuscript.

Funding: This research was funded by the FCT—Fundação para a Ciência e a Tecnologia, Portugal, through the CEOT project UIDB/00631/2020 CEOT BASE and UIDP/00631/2020 CEOT PROGRAMATICO. This work was also developed under the FEDER/Portugal2020 project NIBAP (ALG-01-0247-FEDER-037303).

Institutional Review Board Statement: Not applicable.

Informed Consent Statement: Not applicable.

Data Availability Statement: Not applicable.

Conflicts of Interest: The authors declare no conflict of interest.

References

1. Cima, M.J. Next-generation wearable electronics. *Nat. Biotechnol.* **2014**, *32*, 642–643. [CrossRef] [PubMed]
2. Stoppa, M.; Chiolerio, A. Wearable electronics and smart textiles: A critical review. *Sensors* **2014**, *14*, 11957–11992. [CrossRef] [PubMed]
3. Heo, J.S.; Eom, J.; Kim, Y.-H.; Park, S.K. Recent Progress of Textile-Based Wearable Electronics: A Comprehensive Review of Materials, Devices, and Applications. *Small* **2017**, *14*, 1–16. [CrossRef] [PubMed]
4. Joo, H.; Lee, Y.; Kim, J.; Yoo, J.-S.; Yoo, S.; Kim, S.; Arya, A.K.; Kim, S.; Choi, S.H.; Lu, N.; et al. Soft implantable drug delivery device integrated wirelessly with wearable devices to treat fatal seizures. *Sci. Adv.* **2021**, *7*, eabd4639. [CrossRef] [PubMed]
5. Matsukawa, R.; Miyamoto, A.; Yokota, T.; Someya, T. Skin Impedance Measurements with Nanomesh Electrodes for Monitoring Skin Hydration. *Adv. Healthc. Mater.* **2020**, *9*, e2001322. [CrossRef] [PubMed]
6. Chung, M.; Fortunato, G.; Radacsi, N. Wearable flexible sweat sensors for healthcare monitoring: A review. *J. R. Soc. Interface* **2019**, *16*, 20190217. [CrossRef] [PubMed]
7. Boutry, C.M.; Kaizawa, Y.; Schroeder, B.C.; Chortos, A.; Legrand, A.; Wang, Z.; Chang, J.; Fox, P.; Bao, Z. A stretchable and biodegradable strain and pressure sensor for orthopaedic application. *Nat. Electron.* **2018**, *1*, 314–321. [CrossRef]
8. Oren, S.; Ceylan, H.; Schnable, P.S.; Dong, L. High-Resolution Patterning and Transferring of Graphene-Based Nanomaterials onto Tape toward Roll-to-Roll Production of Tape-Based Wearable Sensors. *Adv. Mater. Technol.* **2017**, *2*, 1700223. [CrossRef]
9. Giraldo, J.P.; Wu, H.; Newkirk, G.M.; Kruss, S. Nanobiotechnology approaches for engineering smart plant sensors. *Nat. Nanotechnol.* **2019**, *14*, 541–553. [CrossRef] [PubMed]
10. Catini, A.; Papale, L.; Capuano, R.; Pasqualetti, V.; Di Giuseppe, D.; Brizzolara, S.; Tonutti, P.; Di Natale, C. Development of a sensor node for remote monitoring of plants. *Sensors* **2019**, *19*, 4865. [CrossRef] [PubMed]
11. Mizukami, Y.; Sawai, Y.; Yamaguchi, Y. Moisture content measurement of tea leaves by electrical impedance and capacitance. *Biosyst. Eng.* **2006**, *93*, 293–299. [CrossRef]
12. Li, M.Q.; Li, J.Y.; Wei, X.H.; Zhu, W.J. Early diagnosis and monitoring of nitrogen nutrition stress in tomato leaves using electrical impedance spectroscopy. *Int. J. Agric. Biol. Eng.* **2017**, *10*, 194–205. [CrossRef]
13. Diacci, C.; Abedi, T.; Lee, J.W.; Gabrielsson, E.O.; Berggren, M.; Simon, D.T.; Niittylä, T.; Stavrinidou, E. Diurnal in vivo xylem sap glucose and sucrose monitoring using implantable organic electrochemical transistor sensors. *iScience* **2020**, *24*, 101966. [CrossRef] [PubMed]
14. Lopez-Martin, A.J.; Carlosena, A. Sensor signal linearization techniques: A comparative analysis. In Proceedings of the 2013 IEEE 4th Latin American Symposium on Circuits and Systems, LASCAS 2013-Conference Proceedings, Cusco, Peru, 27 February–1 March 2013; IEEE: Piscataway, NJ, USA, 2013; pp. 1–4.
15. Kraska, M. Digital linearization and display of non-linear analog (sensor) signals. In Proceedings of the IEEE Workshop on Automotive Applications of Electronics, Dearborn, MI, USA, 19 October 1988; IEEE: Piscataway, NJ, USA, 1988; pp. 45–51. [CrossRef]
16. Islam, T.; Mukhopadhyay, S.C. Linearization of the sensors characteristics: A review. *Int. J. Smart Sens. Intell. Syst.* **2019**, *12*, 1–21. [CrossRef]
17. Alegria, F.; Moschitta, A.; Carbone, P.; Serra, A.D.C.; Petri, D. Effective ADC linearity testing using sinewaves. *IEEE Trans. Circuits Syst. I Regul. Pap.* **2005**, *52*, 1267–1275. [CrossRef]
18. Gong, Z.; Liu, Z.; Wang, Y.; Gupta, K.; da Silva, C.; Liu, T.; Zheng, Z.H.; Zhang, W.P.; van Lammeren, J.P.M.; Bergveld, H.J.; et al. IC for online EIS in automotive batteries and hybrid architecture for high-current perturbation in low-impedance cells. In Proceedings of the 2018 IEEE Applied Power Electronics Conference and Exposition (APEC), San Antonio, TX, USA, 4–8 March 2018; pp. 1922–1929. [CrossRef]
19. Manfredini, G.; Ria, A.; Bruschi, P.; Gerevini, L.; Vitelli, M.; Molinara, M.; Piotto, M. An ASIC-Based Miniaturized System for Online Multi-Measurand Monitoring of Lithium-Ion Batteries. *Batteries* **2021**, *7*, 45. [CrossRef]
20. Crescentini, M.; De Angelis, A.; Ramilli, R.; De Angelis, G.; Tartagni, M.; Moschitta, A.; Traverso, P.A.; Carbone, P. Online EIS and Diagnostics on Lithium-Ion Batteries by Means of Low-Power Integrated Sensing and Parametric Modeling. *IEEE Trans. Instrum. Meas.* **2020**, *70*, 1–11. [CrossRef]
21. Monteiro, F.D.R.; Stallinga, P. Using an Off-the-Shelf Lock-In Detector for Admittance Spectroscopy in the Study of Plants. *Agric. Sci.* **2020**, *11*, 390–416. [CrossRef]

22. Grassini, S.; Corbellini, S.; Angelini, E.; Ferraris, F.; Parvis, M. Low-cost impedance spectroscopy system based on a logarithmic amplifier. *IEEE Trans. Instrum. Meas.* **2014**, *64*, 1110–1117. [CrossRef]
23. Grassini, S.; Corbellini, S.; Parvis, M.; Angelini, E.P.M.V.; Zucchi, F. A simple Arduino-based EIS system for in situ corrosion monitoring of metallic works of art. *Measurement* **2018**, *114*, 508–514. [CrossRef]
24. Campbell, S. How to Make and Arduino Capacitance Meter. Available online: https://www.circuitbasics.com/how-to-make-an-arduino-capacitance-meter/ (accessed on 17 March 2021).
25. Viraktamath, S.V.; Kannur, K.; Kinagi, B.; Shinde, V.R. Digital LCR meter using arduino. In Proceedings of the 2017 International Conference on Computing Methodologies and Communication (ICCMC), Erode, India, 18-19 July 2017; pp. 805–808. [CrossRef]
26. MICROCHIP. *8-Bit AVR Microcontroller with 32K Bytes In-System Programmable Flash, ATmega328P DATASHEET, Rev.: 7810D–AVR–01/15*; Microchip Technology Inc.: Chandler, AZ, USA, 2015.
27. MICROCHIP. *8-Bit Microcontroller with 16/32K Bytes of ISP Flash and USB Controller, ATmega16U4/ATmega32U4 DATASHEET, Rev.: Atmel-7766I-USB-ATmega16U4-32U4 07/2015*; Microchip Technology Inc.: Chandler, AZ, USA, 2015.